Molecular Models of Site-Isolated Cobalt, Rhodium, and Iridium Catalysts Supported on Zeolites: Ligand Bond Dissociation Energies

Mingyang Chen,[a,b] Pedro Serna,[c] Jing Lu,[c] Bruce C. Gates,[c] and David A. Dixon [a,*]

[a] Department of Chemistry, The University of Alabama, Shelby Hall, Box 87036, Tuscaloosa, Alabama 35487-0336, United States
[b] National Center for Computational Sciences, Oak Ridge National Laboratory, Oak Ridge, Tennessee, 37831, USA
[c] Department of Chemical Engineering and Materials Science, University of California, Davis, One Shields Ave, Davis, CA, 95616, United States

Abstract

The chemistry of zeolite-supported site-isolated cobalt, rhodium, and iridium complexes that are essentially molecular was investigated with density functional theory (DFT) and the results compared with experimentally determined spectra characterizing rhodium and iridium species formed by the reactions of $Rh(C_2H_4)_2(acac)$ and $Ir(C_2H_4)_2(acac)$ (acac = acetylacetonate) with acidic zeolites such as dealuminated HY zeolite. The experimental results characterize ligand exchange reactions and catalytic reactions of adsorbed ligands, including olefin hydrogenation and dimerization. Two molecular models were used to characterize various binding sites of the metal complexes in the zeolites, and the agreement between experimental and calculated infrared frequencies and metal–ligand distances determined by extended X-ray absorption fine structure spectroscopy was generally very good. The calculated structures and energies indicate a metal–support-oxygen (M(I)–O) coordination number of two for most of the supported complexes and a value of three when the ligands include the radicals C_2H_5 or H. The results characterizing various isomers of the supported metal complexes incorporating hydrocarbon ligands indicate that some carbene and carbyne ligands could form. Ligand bond dissociation energies (LDEs) are reported to explain the observed reactivity trends. The experimental observations of a stronger M–CO bond than M–(C_2H_4) bond for both Ir and Rh match the calculated LDEs, which show that the single-ligand LDEs of the mono and dual-ligand complexes for CO are ~12 and ~15 kcal/mol higher in energy (when the metal is Rh) and ~17 and ~20 kcal/mol higher (when the metal is Ir) than the single-ligand LDEs of the mono and dual ligand complexes for C_2H_4, respectively. The results provide a foundation for the prediction of the catalytic properties of numerous supported metal complexes, as summarized in detail here.

Key words zeolite supported catalysts; Group 9 transition metals; density functional theory; ONIOM; olefin hydrogenation

* Corresponding author.
E-mail address: dadixon@ua.edu (D. A. Dixon)

1. Introduction

Numerous zeolite- and oxide-supported metal complexes, an important class of catalysts, have been prepared from precursors incorporating metals with formal charges of +1 or +2 reacting with the acidic sites of the supports. Thoroughly investigated materials in this class include Group 9 metals on zeolite HY,[1,2,3,4] Ir, Rh, and Ru complexes on zeolite Hβ,[5,6] and Ir complexes on zeolite HSSZ-53.[7] The Si/Al atomic ratios of the zeolites were chosen to be high (Si/Al = 30, 18, and 24, for zeolites Y, β, and SSZ-53,[7,8,9] respectively) to allow formation of widely separated supported mononuclear species isolated at the Al sites. The nearly unique, well-defined structures of some of these site-isolated supported species were demonstrated by images of the isolated metal atoms obtained with high-resolution aberration-corrected scanning transmission electron microcopy.

This novel class of catalysts offers the advantages of both soluble and supported catalysts that are highly uniform and essentially molecular.[9,10] These advantages may include both high catalytic activity and selectivity.[11] For example, Rh(I) and Ir(I) are highly active metal centers in catalysts for numerous reactions[12,13,14,15] including olefin hydrogenation, C–C bond formation, C–H bond activation, and N–H bond activation. Comparisons of the rate of ethylene hydrogenation catalyzed by dealuminated Y zeolite (DAY zeolite)-supported Ir complexes and by isostructural Ir complexes on other supports demonstrate the important role of the acidic zeolite Al sites as binding sites that withdraw electron density from the metal, enhancing the capability of the sites for dissociating H_2 in the presence of the olefin and thereby facilitating C=C bond hydrogenation.[16] An Ir complex supported on zeolite DAY was found to be ~35 times more active than the isostructural Rh complex on that support.[9] Complexes of Rh and of Ru on zeolite HY used to convert ethylene in the presence of H_2 have been found to have high selectivities for dimerization, forming butenes much more rapidly than ethane.[1c, 17, 18] More complicated reactions are also catalyzed by such supported metal complexes, including, for example, cyclotrimerization of acetylene to form benzene catalyzed by DAY zeolite-supported Rh complexes.[19]

The high degree of uniformity and structural simplicity of the metal complexes in these catalysts commend them to deeper investigation by computational theory and experiment,[20] and in the following we summarize the results of calculations that provide new insights into the chemistry of supported Co, Rh, and Ir complexes. The new results provide strong confirmation of the reported experimental values characterizing the structure and bonding in these essentially molecular surface species.

The comparisons with experiment focus our attention on samples characterized by infrared (IR) and extended X-ray absorption fine structure (EXAFS) spectroscopy as well as atomic-resolution microscopy. Such samples include those on zeolite DAY formed from the precursors $M(L)_2(acac)_{1\text{-}2}$ (acac = acetylacetonate), with M = Ir, Rh, Ru, or Au and the ligands L = C_2H_4, CO, or CH_3. The experimental results led to the conclusion that the metal centers become bonded to the zeolite upon removal of an acac ligand by substitution from a proton on the strong Brønsted acidic Al–OH sites of the zeolite.[5,7,8,9] EXAFS and IR spectra of supported metal complexes that incorporate two CO ligands (metal *gem*-dicarbonyls) confirm that the metal–support-oxygen bonds form at the zeolite Al sites; the sharp, intense ν_{CO} bands are significantly blue-shifted relative to those of the unsupported organometallic precursors,[5,7,8,9] indicating that the binding sites withdraw electron density from the metals,[21,22] as expected for the strongly acidic Al binding sites.

EXAFS data showing the interactions between supported species formed from $Rh^{I}(CO)_2(acac)$ and zeolite DAY indicate that the metal bonds to the acidic sites of the zeolite via two or three Rh–O bonds, which have been modeled using density functional theory (DFT) by three different ring-like structures.[23] Optimization of the structures led to one structure with two O binding sites on the same Al atom and a second structure with a third O site from a neighboring T (Al or Si) atom. Even when a simpler $Al(OH)_4M$ model was used, DFT calculations with the B3LYP functional gave good agreement with experiment: (a) interatomic distances with optimized geometry parameters of $Rh^{I}(C_2H_4)_2$–$Al(OH)_4$, for example, differed by < 0.05 Å from the EXAFS values[19] and (b) scaled vibrational frequencies in most cases agreed within 10 cm^{-1} with the experimental IR values.[20]

Experimental investigations of zeolite-supported metal complexes were recently extended to zeolites other than zeolite Y, including zeolite β.[5] A larger model system, $Al(OR)_4M$, was used in a computational investigation of the Rh and Ru complexes on the β zeolite, where R is either H or a silanol group.[24] A third binding site could be derived from a silanol anion group in the vicinity of the Al atom and, for M^{II} complexes, such as Ru(II) and Os(II) complexes, the anion is needed for charge balance.

The adsorption of N_2, CO and H_2 on structurally well-defined dealuminated HY zeolite-supported iridium diethylene complexes has also been investigated experimentally and computationally at the DFT level with the B3LYP functional.[25] Four different models for the zeolite acid site were used, a simple Ir–$Al(OH)_4$ model, the Ir–$Al(OSi(OH)_3)_4^-$ model, and two large cluster models derived from the zeolite Y crystal structure,[26] with each terminal O atom capped by an H atom and one Ir atom at the acid site. The larger cluster models two structures as Zeo(24-T)Ir with 109 atoms and Zeo(48-T)Ir with 181 atoms where T is the number of Si and Al atoms. The calculations on the Zeo(48-T)Ir were done in the ONIOM approach with only a portion of the model treated at the B3LYP level with the remainder at the Pm6 level. The calculated frequencies with the three smaller models are all larger and in good agreement with experiment in contrast with the DFT/ONIOM calculations for the largest model which are smaller than experiment. The latter result was attributed to issues with the PM6 parameters used for the lower level part of the ONIOM calculations. The results showed that the Ir–$Al(OH)_4$ and Ir–$Al(OSi(OH)_3)_4^-$ models gave similar results for the ligand dissociation energies as long as the geometries remained the same, and both gave good agreement with the largest Zeo(48-T)Ir model. For the largest model, the issues with the PM6 parameters in the ONIOM calculations tend to cancel in the reactants and products in the LDE calculations. The intermediate Zeo(24-T)Ir model differs from the others in some cases due to the structure of the mono-ligand complexes.

This work was further extended to an experimental and computational study of CO, H_2, and C_2H_4 with single sites of Ir in a zeolite.[27] In this second study, the computational work was performed with the Ir–$Al(OH)_4$ and Zeo(48-T)Ir models. For the calculations on the small model, the aug-cc-pVDZ(-PP for Ir) basis set was used and for the larger model a double-ζ basis set with ECPs on all atoms was used with the B3LYP functional. Both models gave good agreement with the experimental frequencies. The LDEs calculated for the simple Ir–$Al(OH)_4$ model and the Zeo(48-T)Ir model are in excellent agreement and further demonstrate that the ligand dissociation energies are dominated by the single metal local site interactions. It is important to note that the LDEs are not small, usually > 40 kcal/mol and in some cases as high as 80 kcal/mol. This is relevant as it means that the ligands under study are strongly interacting with the local metal site, so that weak interactions with the rest of the zeolite are not important in

determining either the ligand vibrational frequencies or the LDEs.

Questions about the reactivities and catalytic properties of such supported metal complexes motivated the research reported here. Specific questions remaining to be addressed include why the reactivity of ethylene on zeolite-supported Ir complexes is higher than that of ethylene on the isostructural Rh complexes. To address this and related issues, we calculated the adsorption energies of a family of ligands on models of zeolite-supported Co, Rh, and Ir complexes. The calculated results are compared with experimental results, especially IR spectra, which have been useful for the identification of the species formed in catalytic reactions.[8] The DFT vibrational frequencies were found to be highly accurate in representing the band assignments.[19,20,25,27] Some critical bands in the C–H and C=O stretching regions are difficult to resolve, because these bands can be slightly shifted in the presence of a second ligand on the metal. DFT isotopic frequency calculations combined with IR spectra of the isotopically labeled species have been found to distinguish these vibrational bands in a number of cases.[20,23]

We have reported the ligand bond dissociation energies (LDEs) for a range of ligands including H, H_2, CO, N_2, C_2H_4, and C_2H_5 on the zeolite-supported species represented as Rh(I)–$Al(OH)_4$ (1),[20]

$$M(L_1)(L_2)–Al(OH)_4 \rightarrow M(L_1)–Al(OH)_4 + L_2 \quad (1)$$

with the LDE given by eq. (2):

$$LDE = E(M(L_1)–Al(OH)_4) + E(L_2) – E(M(L_1)(L_2)–Al(OH)_4) \quad (2)$$

We have also reported the LDEs for N_2, CO, H_2, and C_2H_4 on different models of Ir binding to the acid site in a zeolite. [25,27] In the work reported here, we provide a complete set of LDEs for Co, Rh, and Ir. We also further compare the experimental and calculated vibrational frequencies of the ligands to provide information about the structural uniformity of the samples and the appropriateness of the choice of the models of the supports. The calculated potential energy surface (PES) values for a relatively simple catalytic test reaction, ethylene hydrogenation, on the M(I)–$Al(OH)_4$ sites, show how the choice of metal influences the chemistry, with various intermediates found for the various metals.

In the present work, we studied the binding of various ligands on the acidic site of the zeolite supported Co, Rh and Ir catalysts with two different structural models, including a range of common hydrocarbon ligands and small gas molecules. In particular, we describe the different behaviors of the metal-ethylene (section 3.2) and metal-hydrogen (section 3.3) bonding on the three metal catalyst centers, which shows significant implication for the catalysis of the hydrogenation of ethylene . In addition, we studied the stability of the carbene and carbyne complexes on the three metal centers (section 3.4), as such complexes could be involved in the ethylene activation process as potential intermediates. In sections 3.5 and 3.6, we present the calculated energetics for ligand adsorption for the Ir, Rh, and Co catalysts as well as the the vibrational frequencies characterizing the intermediates to provide direct connections to experiments. The theoretically predicted potential energy surfaces of the ethylene hydrogenation reaction on the zeolite supported catalysts are given in section 3.7. The discussion of the calculated results provides relationships to the available experiments, especially the ethylene hydrogenation reactions on the catalysts.

2. Computational Methods

We employed two models in this study, a simple model of the acid site $Al(OH)_4M$ (Figure 1) and a more extended model (Figure 2). We chose the simple model on the basis of our previous

investigations which showed that this model provided appropriate values for the energetics, structures, and spectral properties in comparison with experiment and with larger models. We used the simple model to investigate the effects of changing the metal from Ir to Rh to Co. The binding of a variety of ligands and pairs of these ligands was investigated in the current work. The ligands include H, H_2, CO, N_2, C_2H_2, C_2H_4, $CHCH_3$, and C_2H_5; these were chosen because they are relevant to the comparison experiments and to catalysis. Open-shell calculations were done in the spin unrestricted formalism. Geometry optimization and second-derivative frequency calculations of the ML_n–$Al(OH)_4$ complexes were done by using DFT with the B3LYP exchange-correlation functional,[28,29,30] the aug-cc-pVDZ basis sets[31] on H, C, N, O, and Al, and the aug-cc-pVDZ-pp basis set and appropriate pseudopotential[32] on Co, Rh, and Ir. We label this combination of basis sets as aug-cc-pVDZ-(pp). This simple model representing the surface sites was chosen because of the large number of calculations to be done and the fact that that this simple model provides good agreement with the structural and vibrational frequency measurements determined by experiment for Rh and Ir in the acid site of a zeolite and good agreement for the LDEs.[20,25,27] The choice of the electronic structure method is that used for the Rh complexes, which consistently showed good agreement between calculated and experimental values.[20] The -D3 version of Grimme's empirical dispersion with the original -D3 damping function[33] was used to check and where needed to correct the LDEs for the $Co(L_1)(L_2)$–$Al(OH)_4$ complexes, as the Co-ligand binding energies are generally much weaker than the Rh-lignad and Ir-ligand bonding.

Although a third binding site is typically not important for the Rh^I and Ir^I complexes, we included the possibility of bonding of the Rh^I and Ir^I species on a 3O site to predict the barrier to conversion between candidate structures suggested by the EXAFS spectra of $Rh^I(CO)_2$ species on DAY zeolite. Structures incorporating $3O_{short}$ structures were calculated by using the $Al(OH)_4M$ model with Rh or Ir anchored at three-hollow sites of $Al(OH)_4^-$ to form an umbrella-like species (see Figure 1 for details). The umbrella-like model qualitatively represents the environment of the 3O site in zeolite-supported metal catalysts.

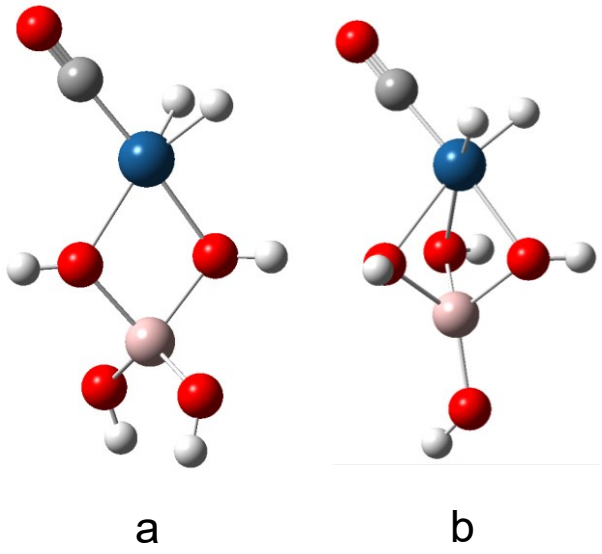

Figure 1. $Ir(CO)(H_2)$ on (a) 2O and (b) 3O sites of $Al(OH)_4^-$. Cyan: iridium. Red: oxygen. Grey: carbon. White: hydrogen.

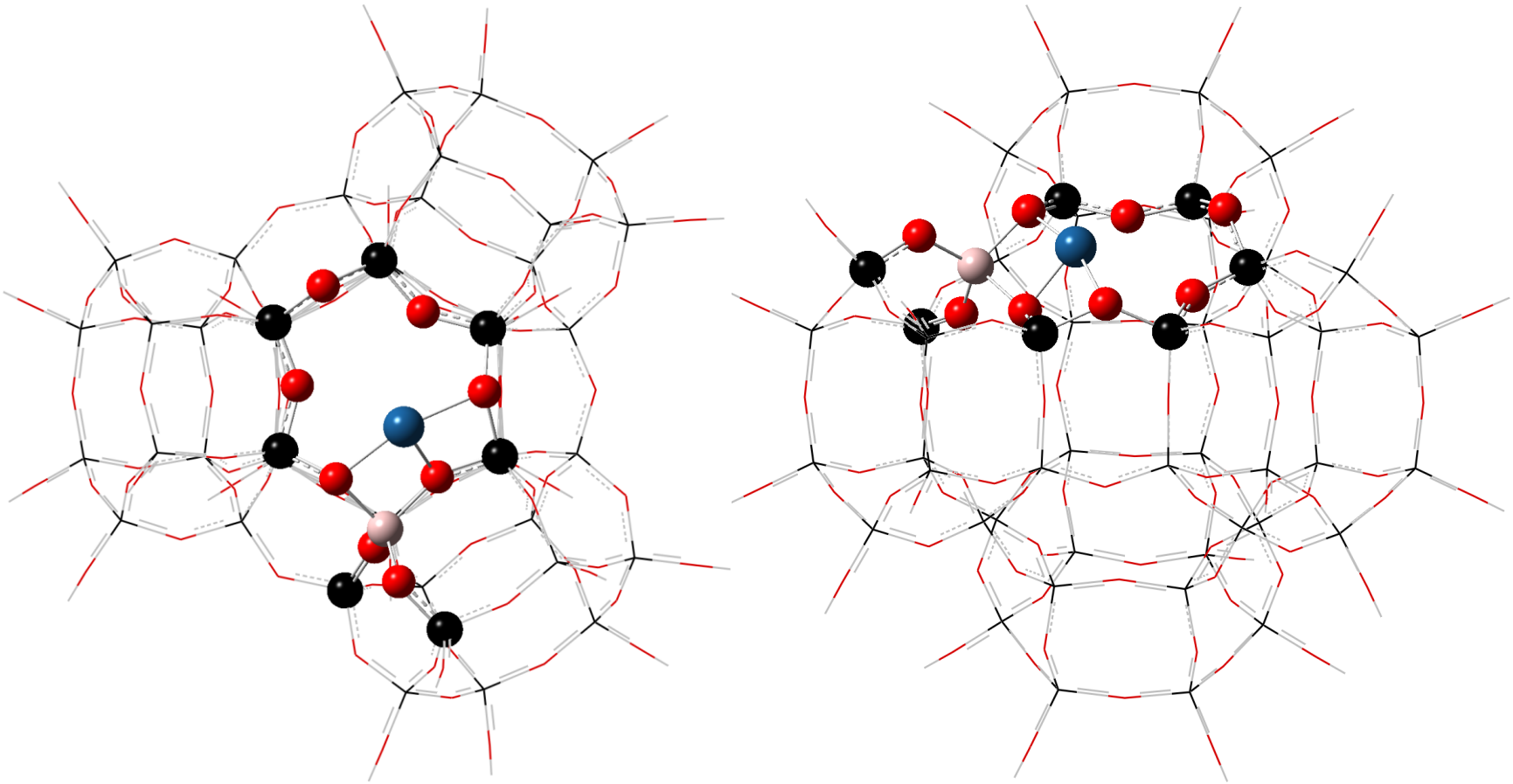

Figure 2. The Zeo(48-T)Ir model for the zeolite-supported Ir catalyst. The high layer is displayed in “ball and bond” mode, and the low layer is displayed as a wire frame. Cyan: iridium. Red: oxygen. Black: silicon.

We used the Zeo(48-T)Ir model to better understand any effects missing from the simple model and to examine the potential effects of longer-range interactions in the zeolite. The acidic center, Al, and the metal catalyst site, Ir, were placed on a 12-member ring, as the 12-member ring is part of the wall of the zeolite supercage. The entire supercage is not included in the calculation because of the high computational cost and because the upper part of the supercage is expected to have only small effects on the ligand binding to Ir, especially in our case, for which the ligands are all very small. We used the ONIOM[34] (our own n-layered integrated molecular orbital and molecular mechanics) hybrid method, which allows ab-initio and semi-empirical molecular orbital and density functional theory methods to be applied to different parts of the molecular system. In the ONIOM calculations, the "high-level" calculation layer comprises the 12-membered ring, two Si–O– groups on the Al, and Ir(L_1)(L_2). The remainder of the system was treated as the "low-level" calculation layer. The "high-level" calculation was done at the DFTlevel with the B3LYP exchange-correlation functional and the cc-pVDZ basis set on the main group elements[35] and the ECPs and basis sets without diffuse functions from above.[32] The "low-level" calculation was performed by using the semi-empirical PM6 molecular orbital method. We chose to use PM6 to perform the "low-level" calculations due to the the most recent parameters available for iridium at the teime the work was initiated which was PM6.

All of the calculations were done by using the Gaussian 09 program system.[36]

3. Results

A comparison of the various Group 9 metal complexes provides an understanding of the periodicity of ligand binding to them. The relative energies of the various isomers for a given pair of ligands are given in the Supporting Information as is the matrix of ligands (L_1 and L_2) and their total ligand dissociation energies (LDEs). EXAFS spectra and previously reported computational results characterizing the zeolite-supported metal complexes with various ligands, including Rh$(CO)_2$, Rh$(C_2H_4)_2$, Ir$(CO)_2$, and Ir$(C_2H_4)_2$ supported on zeolites Y, β, SSZ-53, and SSZ-42[5,7,8,9, 37,38] (each in the hydrogen form [e.g., HY zeolite]) indicate that the zeolite-anchored Rh(I) or Ir(I) center bonds to 2 terminal O atoms at the acidic Al site with M^+ replacing a proton, which is why we chose the simplest model to be M^+–Al$(OH)_4^-$). Most of the Rh(L_1)(L_2)–Al$(OH)_4$ structures with Rh were taken from our previous work,[20] with L = C_2H_4, C_2H_5, CO, N_2, H, and H_2. Additional ligands, such as C_2H_2 and other hydrocarbons, were investigated in the present work, which also extends the earlier work to zeolite-anchored complexes of Co and Ir with the same set of ligands, including the new ligands. The results for the optimized geometries for M(L_1)(L_2)–Al$(OH)_4$ (M = Co, Rh, and Ir) at the B3LYP/aug-cc-pVDZ(-pp) level are shown in the Supporting Information.

As noted above, the simple model of the acid binding site works well in comparison to the much larger Zeo(48-T)Ir(L_1)(L_2) model and to experiment.[25,27] Most of the optimized dual-ligand Zeo(48-T)Ir(L_1)(L_2) complexes and the optimized mono η^2 ligand Ir(L) complexes were found to form bonds with two O atoms on Al with the distance r(Ir–O) equal to ~ 2.1 Å. This result essentially matches EXAFS and computational results for the zeolite-supported metal complexes,[5,7,8,9,37,38] which indicate that the metal center bonds to 2 terminal O atoms of the acidic Al site with M^+ replacing a proton. DFT calculations without using ONIOM show that even for the mono ligand complex, Zeo(48-T)Ir(C_2H_4) that the 2O site is slightly more stable than the 3O site.[27]

The results for the Zeo(48-T)Ir model are completely consistent with those of the simpler

model. The next nearest O atom, from the adjacent Si–O–Si, is ~3 Å from the Ir. The mono η^1 ligand Ir(L) complexes except Ir(C_2H_5) were bonded to 2 O atoms on Al and a O atom on the neighbor Si with r(Ir–O) = 2.1 ~ 2.2 Å. Zeo(48-T)(H_2) and Zeo(48-T)(H_3) also have 3 O atoms bonded to Ir. The addition of the third O atom completes the coordination environment about the Ir. Most of the Zeo(48-T)Ir(L_1)(L_2) complexes with two ligands and two O atoms around the metal display a square-planar or pseudo-square-planar geometry, and so do most of the mono-ligand Zeo(48-T)Ir(L) complexes with 3 O atoms bonded to Ir. Both of the singlet and triplet states of Zeo(48-T)Ir have Ir bonded to 3 O atoms.

The optimized low-spin Ir(L_1)(L_2)–Al(OH)$_4$ geometries are consistent with the optimized Zeo(48-T)(L_1)(L_2) geometries, especially for the dual-ligand complexes. The major difference between the optimized geometries of these two models is that the Ir is in the O–Al–O plane in the Al(OH)$_4$ model, whereas the Ir is out of the O–Al–O plane with an Ir–OO–Al dihedral angle of 30–40° in the Zeo(48-T)Ir model. This difference is attributed to the additional geometry constraints in the larger model. In the calculations for the mono ligand Ir complexes using the larger model, an O atom from a neighboring Si can form a bond with Ir to fill the empty position, found by the Al(OH)$_4$ model to give square-planar coordination at the Ir.

3.1 Spin states of M(L_1)(L_2)–Al(OH)$_4$ complexes

In the cases for which the metal (Co, Rh, Ir) incorporates an even total number of radical ligands such as C_2H_5 and H, the entire molecule can be in a singlet or triplet state; with an odd number of radical ligands, it is in a doublet or a quartet state (Values of S^2 are given in the Supporting Information. Most of the values are in excellent agreement with the expected values showing the presence of little to very modest amounts of spin contamination). Both the low- (singlet/doublet) and high-spin (triplet/quartet) states for all of the Co, Rh, and Ir complexes were investigated. The quintet/sextet states of the Co complexes were also investigated, but none of them is the ground state for the complexes we analyzed. The low-spin Rh and Ir species are always ground states except for Rh–Al(OH)$_4$, Ir–Al(OH)$_4$, Ir(C_2H_5)–Al(OH)$_4$, and Ir(C_2H_5)(H)–Al(OH)$_4$. The Co complexes are mostly high-spin, except for Co(CO)(H)–Al(OH)$_4$ and Co(CO)(C_2H_5)–Al(OH)$_4$, which are ground state doublets by a few kcal/mol. The natural bond orbital (NBO) analysis[39,40,41,42] shows that the low-spin Rh and Ir complexes have the α and β valence d electrons maximally paired, whereas the high-spin Co complexes have the valence d orbitals half occupied (Supporting Information). This type of behavior is also observed in the metal oxides of Cr, Mo, and W.[43,44]

The M–Al(OH)$_4$ complexes have similar geometries. Low-spin Ir–Al(OH)$_4$ complexes with two ligands and two oxygen atoms around the metal normally display a square-planar or pseudo-square-planar geometry, and most of the mono-ligand compounds have the ligand and two oxygen atoms of the zeolite framework filling three of the four square-planar corner positions. Structures with the metal bonded to three oxygen atoms were also investigated but were found to be less stable for most ligands, consistent with the adsorption mode generally accepted on the basis of the EXAFS results.[8,10,18]

The high-spin triplets and quartets have non-planar ligand coordination around the metal, being tetrahedral when two ligands are present and octahedral AX_3E_3 (with X in one axial and two equatorial positions) for the mono ligand complexes. This result is consistent with ligand field theory arguments showing that tetrahedral coordination gives rise to only small d orbital splitting, so that the d occupation of the transition metal remains high-spin.[45] These results are

consistent with the reported IR and DFT results indicating that $Co(CO)_4^+$ is a C_{2v} structure that is Jahn-Teller distorted from the T_d structure,[46] in contrast to the square-planar geometry of $Rh(CO)_4^+$ found by single-crystal X-ray diffraction crystallography.[47] No experimental results are available for $Ir(CO)_4^+$.

The atomic ground state for Co^+ is the ^3F derived from the d^8 configuration, with the ^3F derived from the d^7s^1 being 9.6 kcal/mol higher in energy.[48] The high-spin $Co(L_1)(L_2)–Al(OH)_4$ ground-state structures likely arise from the d^7s^1 excited state of Co^+, which has four unpaired electrons. The ground state of Rh^+ is the ^3F derived from the d^8 electron configuration, with all of the excited states derived from the d^8 configuration lying within 40 kcal/mol of the ground state. The ground state configuration of Rh^+ has only two unpaired electrons, and the low-spin character of $Rh(L_1)(L_2)–Al(OH)_4$ is derived from it. Ir^+ has a ^5F ground state derived from the d^7s^1 configuration, with the ^3F and ^3P states derived from the d^8 configuration being 6.5 and 8.8 kcal/mol higher in energy, respectively. The d^8 excited states give rise to the low-spin character of $Ir(L_1)(L_2)–Al(OH)_4$.

3.2 ethylene species

The ethylene ligand can be adsorbed to the Ir, Rh, and Co complexes by forming two M-C bonds. The ordering of the M-C bond strength in the ethylene species is Ir-C > Rh-C > Co-C, consistent with the ordering of bond distance r(Ir-C) < r(Rh-C) < r(Co-C) (Supporting Information, Table S8). The stronger Ir-C bonding leads to weaker C-C bonding in the ethylene ligands, as indicated from the longer r(C-C) and lower υ(C–C) in the $Ir(C_2H_4)(L)$ complexes than in the Rh and Co counterparts. This implies that the Ir complex has a larger impact on the C=C double bond in ethylene than in the Rh and Co complexes.

3.3 η^2-Hydrogen and dihydride species

The adsorption of hydrogen appears to be quite different from one metal complex to another. H_2 is bonded to Co in its molecular form (η^2-hydrogen) with an average *r*(H–H) of 0.79 Å and an average *r*(Co–H) of 1.90 Å in the presence of an ancillary ligand (C_2H_4, C_2H_5, N_2 or CO). A slightly elongated *r*(H–H) of 0.87 Å and decreased *r*(Co–H) of 1.60 Å is predicted when η^2-hydrogen is the only ligand. In the Ir complexes, H_2, however, splits and forms a dihydride with the *r*(H–H) bonds elongated to approximately twice the bond length (0.74 Å) of the H_2 molecule.[49] The Ir–H bonds are generally ~0.3 Å shorter than the Co–H bonds, suggesting that H_2 is more strongly bonded to the Ir. The hydrogen ligands on the Rh complexes are a mixture of η^2-hydrogen and a dihydride depending on the ancillary ligand. The H_2 is in the dihydride form when the co-ligand on Rh is CCH_3 or $CHCH_3$, or when H_2 is the only ligand attached to the Rh complex; in both cases *r*(H–H) is greater than 1.5 Å. Otherwise, the H_2 ligand is adsorbed in the elongated molecule form by the Rh complexes with *r*(H–H) averaging ~ 0.95 Å, and *r*(M–H) averaging 1.6 Å.

In the Co complexes, the Co–H_2 bonds indicate predominantly a donor–acceptor interaction between the empty Co valence orbital and the H_2 σ orbital, and the back-donation between Co d and H_2 σ* is weak. In the Ir complexes, the strong back-donation overlap between filled Ir d orbitals and the H_2 σ* orbital leads to the formation of M–H σ bonds.[50] In the Rh complexes, the back-donation interactions are weaker than for Ir, and can be either reinforced or reduced by the ancillary ligands on the metal, which leads to the dihydride and η^2-hydrogen forms of the H_2

ligand, respectively. Furthermore, in the presence of the C_2H_2 co-ligand, both the η^2-hydrogen and dihydride species could be formed with the latter 2.4 kcal/mol higher in energy than the former. The Rh dihydride species may be very close to the transition state species for H_2 splitting and are thus sensitive to the chemical environment. The vibrational frequencies of the H_2 ligands follow the bonding trends. Strong π-donor ligands such as $CHCH_3$, CCH_3, and C_2H_2 can enhance the back-bonding between the metal and H, and strong σ donors such as CO and N_2 decrease the bond strength between metal and H slightly. The C_2H_5 ligand has an even greater impact on the M–H bond strength, as shown by a comparison between their bond lengths and the bond lengths of the metal complexes with a single H_2 ligand.

The NBO analysis of the H_2 species shows that the η^2-hydrogen is bound to the metals by a donor-acceptor bond, whereas the dihydrides form two M–H valence bonds with the metals (Supporting Information). The occupancies of the M–H bonding orbitals of the M–dihydride complexes are between 1.7 and 1.9 electrons. A three-center/two-electron bonding scheme has been used to describe the η^2-hydrogen–metal interactions.[50] As the electron density becomes more localized between the metal and the H atom, the H_2 splits into two separate metal hydrides with *r*(H–H) increasing and *r*(M–H) decreasing.

The results of the calculations are consistent with a number of experimental observations.[51] $Rh(C_2H_4)(C_2H_4)$ and $Ir(C_2H_4)(C_2H_4)$ complexes on zeolite Y dissociate H_2 much faster than Rh(CO)(CO) and Ir(CO)(CO) species, respectively. Indeed, when H_2 flows over the supported ethylene complexes, ethyl ligands form along with the appearance of a new band in the IR spectra ascribed to a metal hydride. Carbonyl ligands on each metal are stable in the presence of H_2 as no hydrides are observed. The reactivities for H_2 dissociation are reduced by more than an order of magnitude when one or more CO ligands is bonded to the metal, and the Ir carbonyl complexes are much less reactive than those with two C_2H_4 ligands. The ethylene ligands in these complexes appear to be resistant to the formation of ethyl ligands. These observations match the DFT prediction that the H–H bond in the Ir complex with C_2H_4 as an auxiliary ligand is weaker than the H–H bond in the Ir complex with CO as an auxiliary ligand, as shown by the calculated bond lengths and vibrational frequencies.

3.4 Organic ligand complexes

$M(C_2H_5)(H)–Al(OR)_4$ species have been proposed as intermediates in the catalytic hydrogenation of ethylene.[16] Our calculations characterizing $M(C_2H_5)(L)–Al(OH)_4$ for M = Rh and Ir show that the optimized geometries can depend on the specific metal. $^1Ir(C_2H_5)–Al(OH)_4$ relaxed into $Ir(CHCH_3)(H)–Al(OH)_4$ or $Ir(C_2H_4)(H)–Al(OH)_4$ on optimization, depending on the initial structure. Catalytic reaction experiments conducted with a flow reactor initially containing $Ir(C_2H_4)(C_2H_4)$ complexes supported on zeolite DAY have shown that contact of this catalyst with a pulse of H_2 at 298 K and 1 bar leads to a fast conversion of the initial π-bonded C_2H_4 species as observed by the disappearance of the CH_2 moiety evidenced in the IR spectrum.[10,52,53] This result suggests that the latter structure, while possible according to our calculations, is relatively unstable. The results of experiments carried out with D_2 instead of H_2 demonstrate the formation of Ir–H species as potential intermediates in the ethylene hydrogenation reaction.[16]**Error! Bookmark not defined.** Calculations for the subsequent addition of a second H to the Ir complexes showed that an initial $^1Ir(C_2H_5)(H)–Al(OH)_4$ structure optimizes to a dihydride structure, $Ir(CHCH_3)(H_2)–Al(OH)_4$.

For C_2H_4 bonded to Zeo(48-T)Ir, the most stable structure is $Zeo(48\text{-}T)Ir(CCH_3)(H)$

(Supporting Information). In all other cases, involving, C_2H_4 with additional ligands, the C_2H_4 moiety forms the lowest energy isomer. The form of the ligands can change during the optimization, usually with H-transfer. For example, the monosubstituted Zeo(48-T)Ir($CHCH_3$) optimized to Zeo(48-T)Ir(CCH_3)(H), but the $CHCH_3$ ligands do not transfer hydrogen in the dual-ligand Zeo(48-T)Ir($CHCH_3$)(L) complexes. The optimized Zeo(48-T)Ir(C_2H_5) has an α-H weakly interacting with Ir in contrast to the smaller model. Such a weak Ir–H interaction was not found in the dual-ligand Zeo(48-T)Ir(C_2H_5)(L) complexes. Again, the rearrangements occur to maintain the coordination environment about the metal with H transfer in addition to the association of a third O. Zeo(48-T)Ir(C_2H_5)(H) optimized into Zeo(48-T)Ir($CHCH_3$)(H_2) where the H_2 is really a dihydride with r(H–H) > 2 Å with one α-H on C_2H_5 transferred to the Ir, just as was found for the smaller model. Additional details are given in the Supporting Information.

C_2H_5 does not dissociate on the single-ligand Rh and Co complexes, and in some cases, a terminal H of C_2H_5 is weakly bonded to Rh or Co, forming an agostic stabilized structure which is intermediate in energy between C_2H_5 and C_2H_4/H. This result is relevant to the single-ligand case as Rh(I)(C_2H_5) is hypothesized to be a reactive intermediate in the catalytic ethylene hydrogenation reaction.[54] In ethylene hydrogenation catalyzed by the Rh complex, the Rh(C_2H_4)(H_2)–zeolite Y is converted to Rh(C_2H_5)(H)–zeolite Y before ethane is released. Thus, the calculated results provide insight beyond the experimental results, as the Rh and Ir complexes seem to be indistinguishable from each other in terms of reaction intermediates on the basis of the available IR and EXAFS spectra, which indicate partial hydrogenation of the ethylene ligands present initially and the formation of hydride ligands on each metal. A key difference between the two metals is that the C_2H_5 ligands on Ir (in contrast to those on Rh) may be converted to give M($CHCH_3$)(H)–Al(OH)$_4$ species. The M(C_2H_4)(H_2)–zeolite Y complexes are the lowest energy minimum on both PES's of the C_2H_4 hydrogenation reactions for M = Ir and Rh. The partially hydrogenated species are transient and thus could not be observed experimentally as a consequence of the energetics. With regard to the Co complex-catalyzed C_2H_4 hydrogenation reaction, Co(C_2H_4)(H_2), Co(C_2H_5)(H), and Co(C_2H_5)–zeolite Y are more nearly comparable to each other as compared to potential energy surfaces (PES's) of the Ir and Rh reactions, and therefore, experiments are expected to yield different results.

We also investigated the adsorption of other alkyl, alkene, carbene, and carbyne isomers on our M(I)–Al(OH)$_4$ model of the zeolite to determine the energy differences and LDEs for the various hydrocarbon isomers. We replaced all of the C_2H_4 ligands in the M(C_2H_4)–Al(OH)$_4$ complexes with $CHCH_3$ ligands, and replaced all the C_2H_5 ligands in the M(C_2H_5)–Al(OH)$_4$ complexes with $CHCH_3$/H ligands, for M = Co, Rh, and Ir (Supporting Information, Table S6). Most of the M($CHCH_3$)(L)–Al(OH)$_4$ complexes are vibrationally stable species, although a few optimize to structures different from the starting one. With regard to the Rh complexes, although C_2H_5 was shown to be a stable ligand, some of its isomers, such as $CHCH_3$/H, can lie close to it in energy, and the IR spectra may not be able to distinguish them. Therefore, we carefully optimized the Co, Rh, and Ir complexes with organic ligands that are possibly formed in rearrangements from C_2H_n or C_2H_n/H_m.

The predictions of the lowest-energy complexes among the complexes with isomeric ligands based on the Ir(L_1)(L_2)–Al(OH)$_4$ model, in general, agree with the predictions made using the Zeo(48-T)Ir(L_1)(L_2) model. One of the exceptions is that the carbyne CCH_3/H ligand groupings (Supporting Information, Figure S3) are the most stable isomer ligands on Ir–Al(OH)$_4$ among the C_2H_4 isomers. The reaction path could be different for the reactions catalyzed by the Ir complexes because the $CHCH_3$ complex is energetically accessible as a reactive intermediate.

For example, $M(C_2H_4)(C_2H_4)$ is calculated to be ~10 kcal/mol more stable than $M(C_2H_4)(CHCH_3)$, so the $CHCH_3$ intermediate with no additional ligand would only be observed at low C_2H_4 concentrations.

Our calculations show that the C_2H_4/L ligands are more stable than their isomeric counterparts on the Ir–$Al(OH)_4$ and Rh–$Al(OH)_4$ complexes in most cases, whereas the mono hydrocarbon ligands such as C_2H_4, C_2H_5, and Z-but-2-ene are more favored by the Co complexes, and $Co(C_2H_4)(L)$ complexes are slightly higher in energy than their lowest isomers. The stabilities of the carbene and carbyne ligands on the various metal complexes are in the order Ir > Rh > Co. The carbene complexes relative to the olefin complexes are substantially more stable than the isolated carbene, for which the triplet carbene, $^3HCCH_3$, is 67.8 kcal/mol higher in energy than the C_2H_4; and the singlet carbene, $^1HCCH_3$, is even higher in energy, 72.5 kcal/mol relative to C_2H_4.

For the Rh complexes, the energy gaps between the complexes with the $CHCH_3$/L ligands (or other most stable carbene ligands) and the lowest-energy isomers are ~ 20 kcal/mol, which is 5 to 10 kcal/mol greater than the gaps between the isostructural Ir complexes. The carbyne complex $Rh(CCH_3)(H)$–$Al(OH)_4$ is 13 kcal/mol higher in energy than the lowest isomeric complex $Rh(C_2H_4)$–$Al(OH)_4$ and 2 kcal/mol more stable than $Rh(CHCH_3)$–$Al(OH)_4$. The energy gaps continue to increase when the $CHCH_3$ ligand is attached to the Co complexes, and structural rearrangements occur in a few cases; for example, $CHCH_3$/$CHCH_3$ combines to form Z-but-2-ene (Supporting Information, Figure S3).

On the basis of the metal–carbon bond lengths and vibrational stretching frequencies (Supporting Information), the bonds between the metal centers M and the carbene/carbyne ligands can be described as metal–carbon double/triple bonds. The values for $W{=}CH_2$ in models of the Schrock complex are r(M–C) = 1.89 Å with υ(M–C) 816 cm^{-1}.[55] The M-C bond lengths are in the range of 1.83–1.87 Å for the Ir complexes incorporating carbene ligands, compared with the average r(Ir–C) = 2.05 Å of the bond in the $Ir(C_2H_5)(L)$–$Al(OH)_4$ complexes. The vibrational frequencies characterizing the metal–carbon stretching modes are in the range of 620 to 720 cm^{-1} in the $Ir(CHCH_3)(L)$–$Al(OH)_4$ complexes, 819 cm^{-1} for CH_2/C_3H_6, and 759 cm^{-1} for the cyclo-IrCHCHCH(CH_3) 4-member ring structure; the values for Ir–C_2H_5 are in the range of 500 to 560 cm^{-1}. The Ir complexes with the β-agostic C_2H_5 ligands are characterized by values of r(Ir–C) and υ(Ir–C) falling between those of the $Ir(C_2H_5)$ and $Ir(CHCH_3)$ complexes, indicating that the Ir–C bonds in the complexes are stronger than an Ir–C single bond and weaker than an Ir–C double bond, consistent with the calculated LDEs, which show that the hydrogen-bonded C_2H_5 ligands are more stable than a 'normal' C_2H_5 when they are attached to the Ir atom. The Ir–carbyne molecule, $Ir(CCH_3)(H)$–$Al(OH)_4$, has a shorter r(Ir–C) (1.70 Å) and a higher υ(Ir–C) (1478 cm^{-1}) than those of the $Ir(CHCH_3)(L)$–$Al(OH)_4$ species.

C_2H_6 can form two weak C–H···Co interactions with Co–$Al(OH)_4$, and it is the lowest-energy isomer of the C_2H_4/H_2 ligand combinations. The adsorption of hydrogen-bonded ethane on the Rh complexes is ~20 kcal/mol more endothermic than the formation of the lowest-energy isomer, $Rh(C_2H_4)(H_2)$–$Al(OH)_4$, but it is stable in terms of the adsorption of C_2H_5/H and $CHCH_3$/H_2. Ethane forms an extremely unstable triplet complex with Ir–$Al(OH)_4$, ~60 kcal/mol higher in energy than the lowest-energy isomeric complex $Ir(C_2H_4)(H_2)$–$Al(OH)_4$.

$M(C_2H_4)(C_2H_4)$–$Al(OH)_4$ is the lowest-energy isomer for M = Rh and Ir but for M = Co, the lowest energy isomer is Co(Z-but-2-ene)–$Al(OH)_4$. Similarly, $M(C_2H_4)(C_2H_5)$–$Al(OH)_4$ is the lowest-energy isomer for M = Ir and Rh, whereas M(*sec*-butyl)–$Al(OH)_4$ is 8.7 kcal/mol lower in energy for M = Co.

3.5 Ligand bond dissociation energies (LDEs) for M(I)(L_1)(L_2)–X (X = $Al(OH)_4$)

To calculate the ligand dissociation energies (reaction (1) and equation (2)), we used the lowest-energy ^{3}M–$Al(OH)_4$ structure. For the dual-ligand Ir complexes (Ir(L_1,L_2)), the average single LDEs (Table 1) are in the order: H ≈ CO > C_2H_5 ≈ C_2H_2 ≈ C_2H_4 > H_2 > N_2. For the dual-ligand Rh complexes, the average single LDEs behave similarly with H > CO > C_2H_5 > C_2H_2 ≈ C_2H_4 > N_2 ≈ H_2. These LDEs are large enough that they will be dominated by the interaction with the metal and the effect of the surrounding ligand environment will be small. For the dual-ligand Co complexes, the average single LDEs are in the order, H > C_2H_5 > CO > C_2H_2 > C_2H_4 > N_2 > H_2, which is similar to those for the Ir and Rh complexes but does show some differences. The corresponding values with the -D3 dispersion corrected functional[33] for the Co complexes show only modest effects for the weak interactions. The impact of the surrounding zeolite environment will be larger for the low LDEs in the Co complexes. The results show that H_2 is unbound or only very weakly bound to the Co, whereas it is more strongly bonded for the Ir and Rh complexes. The average LDEs for the single ligand dissociation follow the trend Ir > Rh > Co. The LDEs of the dual-ligand Ir complexes are ~ 15 kcal/mol greater than the LDEs of the corresponding Rh complexes, and ~50 kcal/mol greater than the LDEs of the corresponding Co complexes, in general. The LDEs of radical ligands such as C_2H_5 and H on the Co complexes are only ~ 25 kcal/mol less than the LDEs of the corresponding Ir complexes.

Table 1. Calculated Average LDEs in kcal/mol for M(L_1,L_2) and M(L) Complexes

Ligand	Ir(L_1,L_2)[a]	Rh(L_1,L_2)	Co(L_1,L_2)[b]	Ir(L)[a]	Rh(L)	Co(L)[a]
H	70/77	59	44(44)	79/	56	72(72)
CO	69/70	50	28(33)	77/71	47	45(45)
C_2H_5	53[c]/59	42	17(20)	/72	54[d]/44	56(58)
C_2H_2	50/54	36	12(16)	87/83	47	49(51)
C_2H_4	49/52	36	9(10)	60/47	35	39(43)
H_2	42/46	27	3(4)	54/45	22	26(27)
N_2	36/41	25	0(1)	45/43	23	19(19)

[a] Values after the slash are for the LDEs calculated with the Zeo(48-T)Ir model. [b] -D3 results in parentheses. [c] M-L LDEs were calculated using the Zeo(48-T)Ir model for Ir(C_2H_5)(L) as Ir(C_2H_5)–$Al(OH)_4$ is not a minimum energy structure. [d] agostic C_2H_5.

For the Ir and Co complexes with one ligand, the metal–ligand bond is much stronger than the bonds in the two-ligand complexes for the same ligand. For the Rh complexes, the bond dissociation energies for the first and second ligands are comparable to each other in most cases. The LDEs characterizing the mono-ligand complexes (in kcal/mol) are as follows: C_2H_2 > H ≈ CO > C_2H_4 > H_2 > N_2 for Ir; H ≈ agostic C_2H_5 > CO ≈ C_2H_2 ≈ C_2H_5 > C_2H_4 > N_2 ≈ H_2 for Rh; and H > C_2H_5 > C_2H_2 > CO > C_2H_4 > N_2 > H_2 for Co. For Co, the corresponding values with the -D3 correction again show only small effects. These energy differences can affect the overall energetics of ligand adsorption and can potentially change the selectivity of the ligand adsorption, especially for the hydrocarbons.

The detailed LDEs for Zeo(48-T)Ir(L) and Zeo(48-T)Ir(L_1)(L_2) are shown in Table S4 (Supporting Information). The LDEs (in kcal/mol) for mono ligand Zeo(48-T)Ir(L) are in the

order: C_2H_2 > C_2H_5 ≈ H ≈ CO > C_2H_4 > H_2 > N_2. For the dual-ligand Zeo(48-T)Ir(L_1)(L_2), the LDEs for a given L are generally lower than the LDEs(L) for the mono ligand complex Zeo(48-T)Ir(L) for most L. In the dual-ligand complexes with C_2H_2 ligands, the LDE for both ligands were significantly lower (by ~ 30 kcal/mol for most Zeo(48-T)Ir(C_2H_2)(L)) than the corresponding LDEs in the mono-ligand complexes. The presence of C_2H_5 also lowers the LDEs in the dual-ligand complexes as compared to the LDEs in the mono-ligand complexes, by ~15 kcal/mol on average, which is smaller than the effect of C_2H_2. The CO ligand in the dual-ligand complexes has a very small effect on the LDEs. Slightly higher LDEs were found for both ligands of most dual- ligand complexes that contain H, H_2, or C_2H_4 than the corresponding LDEs in the mono ligand complexes. The increase in LDEs of the dual-ligand complexes with H, H_2, and C_2H_4 ligands might be attributed to weak interactions between the ligands. These results suggest that in the dual ligand Zeo(48-T)Ir(L_1)(L_2) complexes, the bonding between Ir and the ligand can decrease the LDE for its auxiliary ligand, but this effect can be canceled out by the interaction between the two ligands. The LDE($CHCH_3$) for Zeo(48-T)Ir($CHCH_3$) and LDE(L) for Zeo(48-T)Ir($CHCH_3$)(L) are not shown, because Zeo(48-T)Ir($CHCH_3$) relaxed into Zeo(48-T)Ir(CCH_3)H during the optimization. The bonds between Ir and $CHCH_3$ were found to be very strong in the dual-ligand Zeo(48-T)Ir-($CHCH_3$)(L) complexes, ~ 80 kcal/mol for L = C_2H_2 and ~ 110 kcal/mol for the remaining L's.

The LDEs and total LDEs for Ir(L_1)(L_2)–Al(OH)$_4$ (Supporting Information) are consistent in most cases with the LDEs calculated using the Zeo(48-T)Ir(L_1)(L_2) model, and the energy differences are ~5 kcal/mol for the single-ligand LDE, and <10 kcal/mol for the total LDE with a few exceptions. The C_2H_4 LDE for Ir(C_2H_4) calculated by using the large Zeo(48-T)Ir model is ~13 kcal/mol smaller than using the Ir–Al(OH)$_4$ model, and the H LDE for Ir(C_2H_4)H calculated by using the Zeo(48-T)Ir model is ~14 kcal/mol larger than the value obtained using the Ir–Al(OH)$_4$ model, both of which suggest that the bond between Ir and C_2H_4 in Zeo(48-T)Ir(C_2H_4) is weaker than the Ir–C_2H_4 bond in Ir(C_2H_4)–Al(OH)$_4$. This difference is likely a consequence of the fact that the orientation of the η^2-C_2H_4 in the optimized geometry calculated by using the Zeo(48-T)Ir model is different from that determined by using the Ir–Al(OH)$_4$ model (Supporting Information, Figure S4). In IrC_2H_4–Al(OH)$_4$, the C_2H_4 ligand is approximately in the O–Ir–O plane (i.e., in one of the octahedral positions around Ir), and the C=C bond is perpendicular to the O–Ir–O plane. In Zeo(48-T)Ir(C_2H_4), the C_2H_4 ligand is more bent out of plane, and the C=C bond is no longer perpendicular to the O–Ir–O plane. The distortion of the Ir–C_2H_4 in Zeo(48-T)Ir(C_2H_4) decreases the overlap between the electron densities of Ir and C=C, and thus decreases the C_2H_4 bond energy. This difference is most likely a consequence of a steric effect in the large Zeo(48-T)Ir model, as the η^2 bonding C_2H_4 is relatively bulky relative to the other ligands that were investigated. Although C_2H_2 is also an η^2 bonding ligand, the steric effect for zeolite-supported Ir(C_2H_2) is small (Figure S4). The C_2H_2 ligands are characterized by the same distance to two terminal O atoms on Ir, and the C≡C bond is perpendicular to the O–Ir–O plane determined by each computational model. The stability of the alkyl, carbene and carbyne isomers of the M(C_2H_4)(L) complexes is substantially related to the strength of the M-C bond between M and C_2H_4. The slightly weaker M-C bond predicted by the more realistic Zeo(48-T)Ir model infers that the stability of the alkyl, carbene and carbyne isomer complexes might be somewhat overestimated by using the M–Al(OH)$_4$, but such isomers should still be relevant for ethylene activation.

Considering the much higher computational cost of using the Zeo(48-T)Ir model, the more efficient and reasonably reliable small model is appropriate for the investigation of the large

number of $M(L_1)(L_2)$–$Al(OH)_4$ complexes that we considered. For Ir(CO), Ir(N_2), Ir(H), and Ir(H_2), which were predicted to have one more O atom bonded to Ir on the basis of the Zeo(48-T)Ir model than on the basis of the Ir–$Al(OH)_4$ model, the differences in the LDEs according to the two models were found to be small, suggesting that the additional O atom that is bonded to Ir has only a small influence on the energetics. The average LDE(L_1) values (in kcal/mol) for the dual-ligand Zeo(48-T)Ir(L_1)(L_2), where the remaining ligand L_2 follow the same order as for the simple complex.

3.6 Vibrational frequencies

The calculated vibrational frequencies of the $M(L_1)(L_2)$–$Al(OH)_4$ complexes were scaled by using the ratios between the experimental IR fundamental bands and the B3LYP/aug-cc-pVDZ(-pp) frequencies for the ligand molecules.[56] The C–H stretches of C_2H_2, C_2H_4, C_2H_5, $CHCH_3$, and other hydrocarbon ligands were scaled by a factor of 0.960 on the basis of $\upsilon_{expt}/\upsilon_{dft}$ of C_2H_4 or C_2H_2; the C–O and N-N stretches were scaled by 0.987 and 0.959 on the basis of $\upsilon_{expt}/\upsilon_{dft}$ for molecular CO and N_2; and the Ir–H stretching modes were scaled by a factor of 0.983 on the basis of $\upsilon_{expt}/\upsilon_{dft}$ of H_2. The scaled calculated vibrational frequencies for $M(L_1)(L_2)$–$Al(OH)_4$ are shown in Tables S8-S16 (Supporting Information).

The C–H stretching modes calculated for the Ir–$Al(OH)_4$ complexes are in the range of ~ 2800 to 3000 cm^{-1} for the C_2H_5 ligands (Supporting Information, Table S11), 2900 to 3100 cm^{-1} for the C_2H_4 ligands (Supporting Information, Table S12), and in the 3100+ cm^{-1} region for the C_2H_2 ligands (Supporting Information, Table S13). The C–H stretches characterizing the Rh complexes are ~ 10 to 20 cm^{-1} higher in frequency than those characterizing the Ir complexes with the same ligands, on average. The trend does not hold as well when moving from Rh to Co, but the frequencies of most C–H stretches in the Co complexes are greater than those in the Rh complexes.

The C–O, N–N, and Ir–H stretches characterizing most of the Ir complexes are in the range of 2000 to 2400 cm^{-1} (Supporting Information, Tables S8, S14 and S15). The C–O stretches have very strong intensities, with the frequencies mostly being in the range of ~ 2020 to 2060 cm^{-1} (2095 cm^{-1} for the symmetric or antisymmetric bands in the *gem*-dicarbonyl complex). The C–O stretches in the Rh(CO)(L)–$Al(OH)_4$ are ~10–20 cm^{-1} higher in frequency than the stretches characterizing the Ir complexes, and the frequencies of the CO stretches characterizing the Co complexes are mostly a few tens of cm^{-1} higher than those characterizing the Rh complexes. The N–N stretches characterizing the Ir complexes are found to be in the range of 2140 to 2195 cm^{-1}. Similar to the C–O stretches, the N–N stretches characterizing the Rh and Co complexes are higher than the stretches characterizing the Ir complexes, due to the stronger M-CO/M-N_2 bonding of the Ir complex.

The Ir–H stretching modes range in frequency between 2190 and 2370 cm^{-1} and have moderate intensities. The vibrational frequencies characterizing the M–H stretching modes in the $M(H_2)L$–$Al(OH)_4$ complexes largely depend on the strength of the H_2 3-center-2-electron bond, as discussed above. The frequency of the M–H stretching modes of M(H)(L)–$Al(OH)_4$ decreases from Ir to Rh to Co. The Co(H)(L)–$Al(OH)_4$ complexes are characterized by Co–H stretches of the high-spin species that are significantly lower in frequency than those of the Co–H stretches of the low-spin species. Thus the Co–H stretching frequencies can be used to distinguish the ground states of the Co complexes when there are multiple spin states that are close to each other in energy. The Co complexes with the η^2-hydrogen ligands display high υ(H–H) values in the

region of 3650–4120 cm^{-1}, indicating that the forces between Co and H_2 are weak in comparison with the strength of the H–H bond. The calculated values of υ(H–H) for the η^2-hydrogen ligand Co complexes show red shifts from the calculated harmonic value of 4356 cm^{-1} for molecular H_2 (ν(experiment) = 4159 cm^{-1} with ω_e = 4401.21 cm^{-1} and $\omega_e x_e$ = 121.34 cm^{-1}).[49]

In summary, the Ir complexes have the highest M–L stretching frequencies, and the Co complexes have the lowest frequencies. The vibrational frequencies of the stretching modes in the ligands display a reversed order, with the Ir complexes having the lowest frequencies due to the denser electron density on the Ir-L bonds. This pattern is consistent with the increase of the LDEs from Co to Rh to Ir. The back-donation bond strength increases from Co to Rh to Ir, leading to lower intra-ligand stretching frequencies and larger M–L stretching frequencies. The changes in frequencies can be attributed to the increases of the electron density donated into the molecular orbitals between M and L.

3.7 Hydrocarbon activation reaction potential energy surfaces

The results described in the above six sections characterize the stable stationary points on the potential energy surface. The ethylene hydrogenation reaction catalyzed by the molecular organometallic fragments on zeolites was investigated with the Zeo(48-T)Ir and M–$Al(OH)_4$ models (Figure 3). Reaction energies of -31.7 kcal/mol obtained at the B3LYP/aug-cc-pVDZ(-pp) level and -32.0 kcal/mol obtained at the B3LYP/cc-pVDZ level for the reaction $C_2H_4 + H_2 \rightarrow C_2H_6$ agree well with the reaction energy of -32.6 kcal/mol calculated from the experimental gas-phase enthalpies of formation at 298 K.[57] We investigated the process whereby the metal complex catalyst adsorbs C_2H_4 and H_2 in different order as shown by reactions (5) and (6):

$$H_2 + M(C_2H_4)–Al(OH)_4 \rightarrow C_2H_6 + M–Al(OH)_4 \quad (5)$$

$$C_2H_4 + M(H_2)–Al(OH)_4 \rightarrow C_2H_6 + M–Al(OH)_4 \quad (6)$$

The singlet Ir–$Al(OH)_4$ precursor catalyst is 2.3 kcal/mol higher in energy than the ground state triplet (Figure 3b). The singlet states are lower in energy than the triplet states for the formation of the first-step adsorption products, Ir(C_2H_4)–$Al(OH)_4$ and Ir(H_2)–$Al(OH)_4$, and the singlet-triplet splitting is less than 5 kcal/mol. The singlet-triplet splitting increases to ~ 40 kcal/mol for the second-step adsorption product Ir(C_2H_4)(H_2)–$Al(OH)_4$ (and the rearranged isomer Ir($CHCH_3$)(H_2)–$Al(OH)_4$), and so we can infer that the reaction will proceed on the singlet surface.

The rearranged isomers Ir($CHCH_3$)(H_2)–$Al(OH)_4$ and Ir($CHCH_3$)(H)–$Al(OH)_4$ are more important on the Ir PES than on the Rh and Co PES's. Ir(C_2H_4)–$Al(OH)_4$ can isomerize into Ir(CCH_3/H)–$Al(OH)_4$ exothermically by -16.8 kcal/mol. Ir(C_2H_4)(H_2) rearranges into intermediates including α-H bonded Ir(C_2H_5)(H), β-H bonded Ir(C_2H_5)(H), and Ir($CHCH_3$)(H_2) with the $Al(OH)_4$ model, but only the latter is found using the Zeo(48-T)Ir model. Ir($CHCH_3$)(H_2) is 11.3 kcal/mol higher in energy than Ir(C_2H_4)(H_2) on $Al(OH)_4$, but is more stable than the α-H bonded Ir(C_2H_5)(H) and the β-H bonded Ir(C_2H_5)(H) by a few kcal/mol. If the H's on Ir are not involved in the rearrangement (i.e., intra-ligand) of Ir(C_2H_4)(H_2) to form Ir($CHCH_3$)(H_2), the transition state is predicted to be a bridged Ir($HC\text{-}H\text{-}CH_2$)(H_2) structure, with a barrier of ~70 kcal/mol. The Ir($CHCH_3$)(H_2) can also form by an inter-ligand exchange process where a H on Ir can attack the C of C_2H_4 to break the Ir–C bond and become a β-H in the newly formed ligand. This pathway has a much lower reaction barrier than the intra-ligand H transfer path. With the Ir–$Al(OH)_4$ model, the inter-ligand H transfer possibly forms β-H bonded Ir(C_2H_5)(H) before the formation of Ir($CHCH_3$)(H_2), whereas with the Zeo(48-T)Ir model, Ir(C_2H_5)(H) is no longer

predicted to be a local minimum, and $Ir(CHCH_3)(H_2)$ become the H transfer intermediate. $Ir(CHCH_3)(H_2)$ can also be formed by the addition of H_2 to $Ir(CCH_3)(H)–Al(OH)_4$, with a

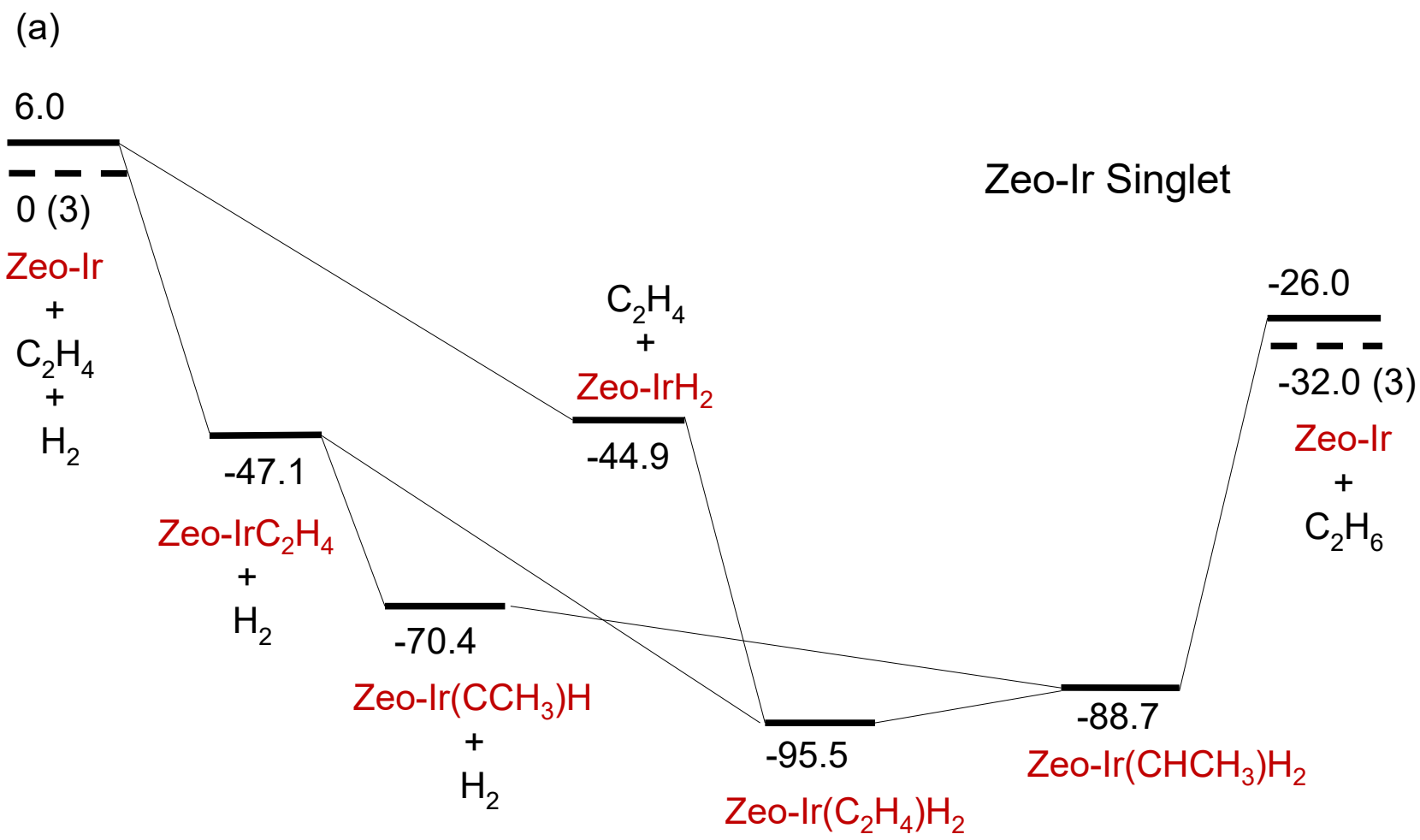
(a)
6.0
0 (3)
Zeo-Ir
+
C2H4
+
H2
-47.1
Zeo-IrC2H4
+
H2
-70.4
Zeo-Ir(CCH3)H
+
H2
C2H4
+
Zeo-IrH2
-44.9
-95.5
Zeo-Ir(C2H4)H2
Zeo-Ir Singlet
-88.7
Zeo-Ir(CHCH3)H2
-26.0
-32.0 (3)
Zeo-Ir
+
C2H6

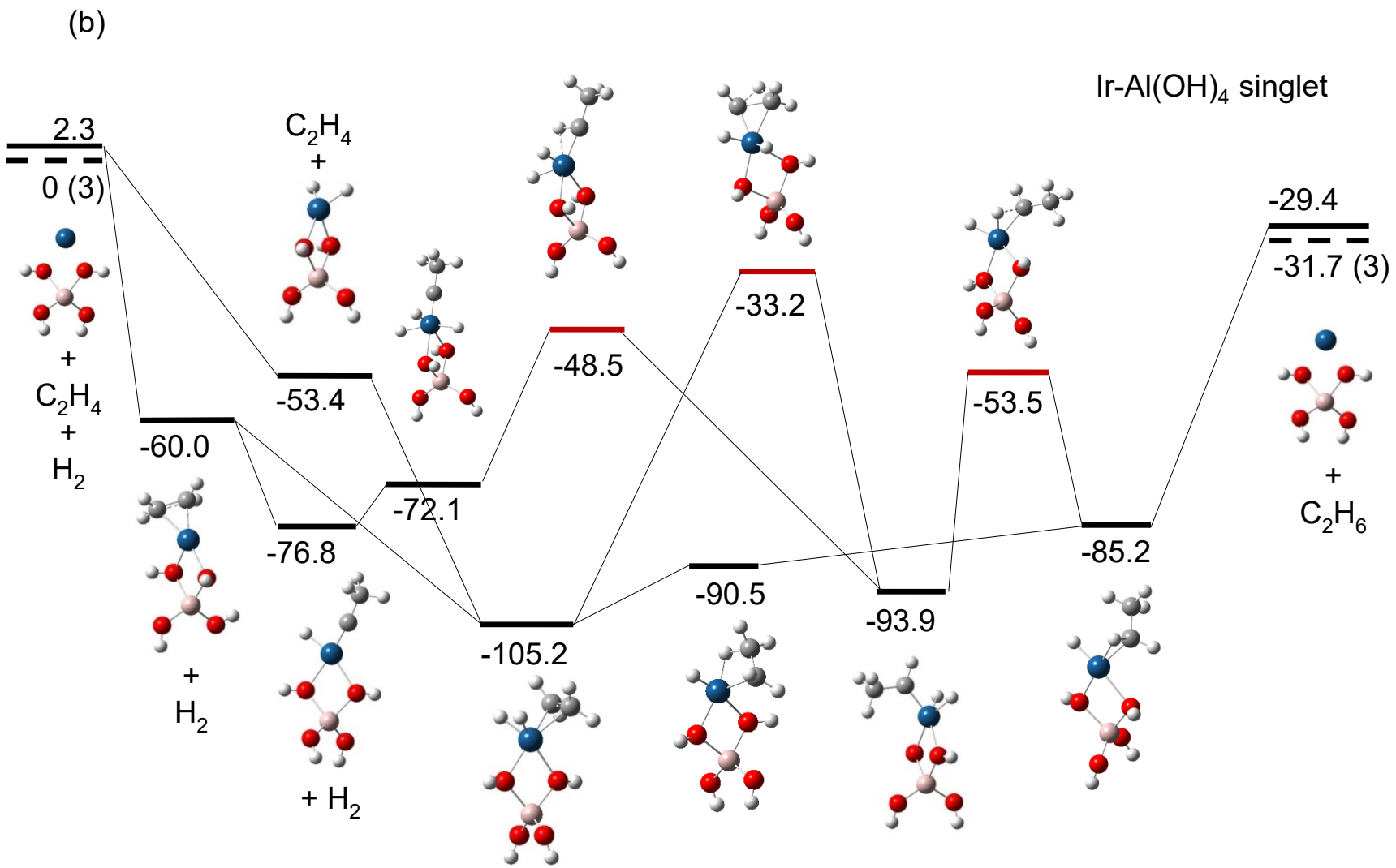
(b)
Ir-Al(OH)4 singlet
2.3
0 (3)
+
C2H4
+
H2
-60.0
+
H2
C2H4
+
-53.4
-76.8
+ H2
-72.1
-48.5
-105.2
-33.2
-90.5
-93.9
-53.5
-85.2
-29.4
-31.7 (3)
+
C2H6

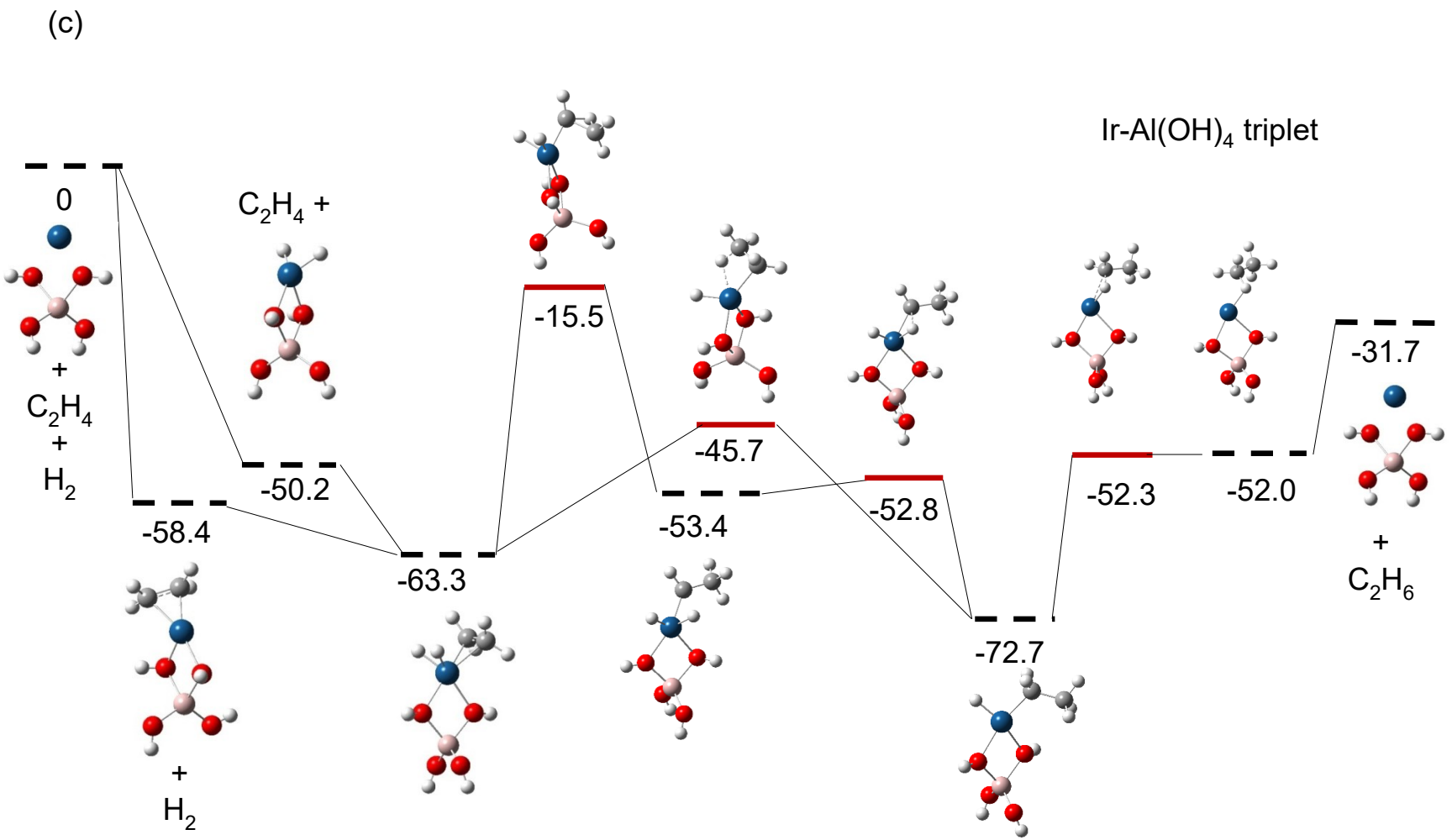
(c)
Ir-Al(OH)4 triplet
0
+
C2H4
+
H2
-58.4
+
H2
C2H4 +
-50.2
-63.3
-15.5
-45.7
-53.4
-52.8
-72.7
-52.3
-52.0
-31.7
+
C2H6

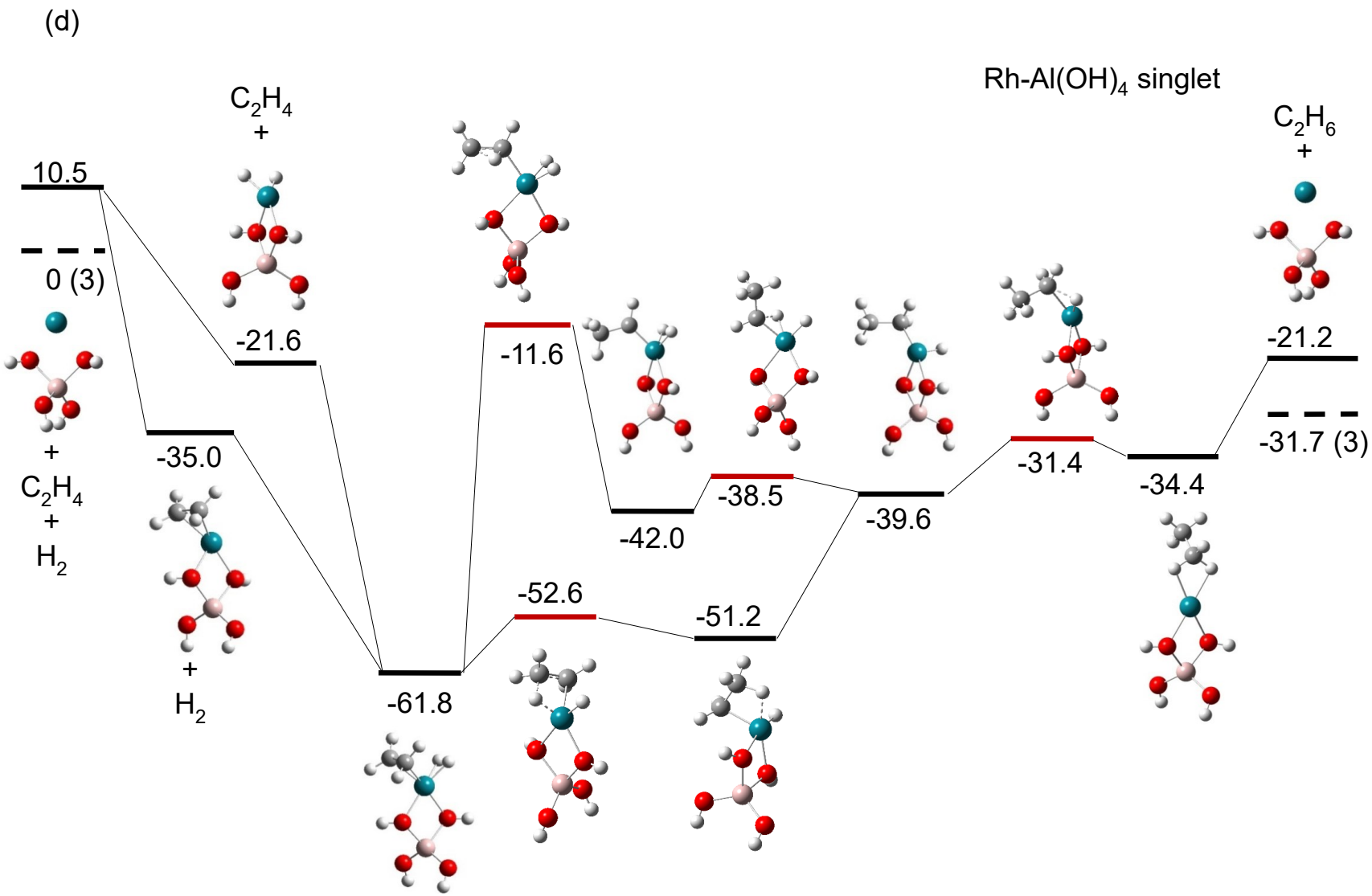
(d)
Rh-Al(OH)4 singlet
C2H4
+
10.5
0 (3)
+
C2H4
+
H2
-21.6
-35.0
+
H2
-61.8
-11.6
-52.6
-42.0
-38.5
-51.2
-39.6
-31.4
-34.4
C2H6
+
-21.2
-31.7 (3)

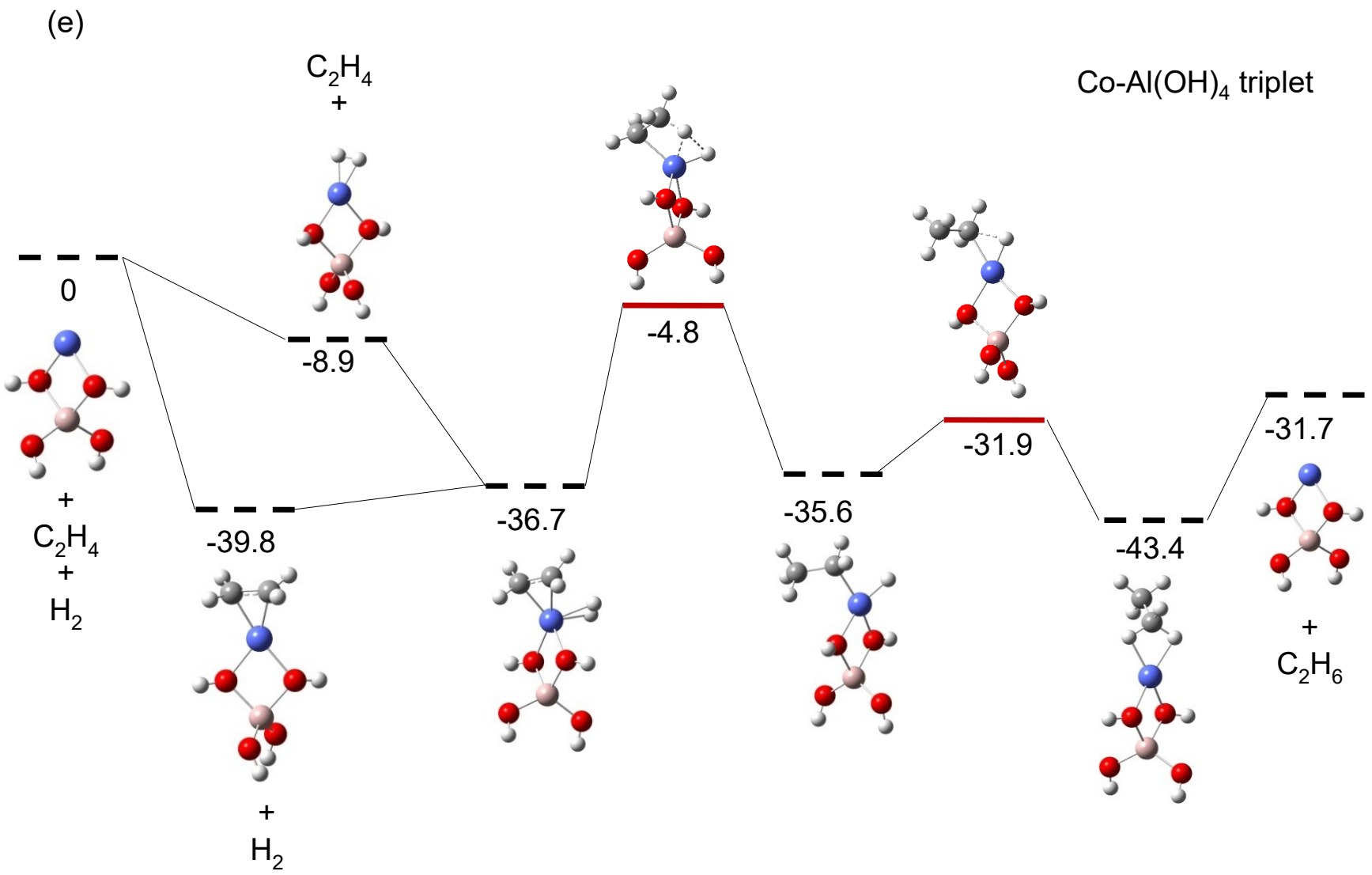
(e)
Co-Al(OH)4 triplet
C2H4
+
0
+
C2H4
+
H2
-8.9
-39.8
+
H2
-36.7
-4.8
-35.6
-31.9
-43.4
-31.7
+
C2H6

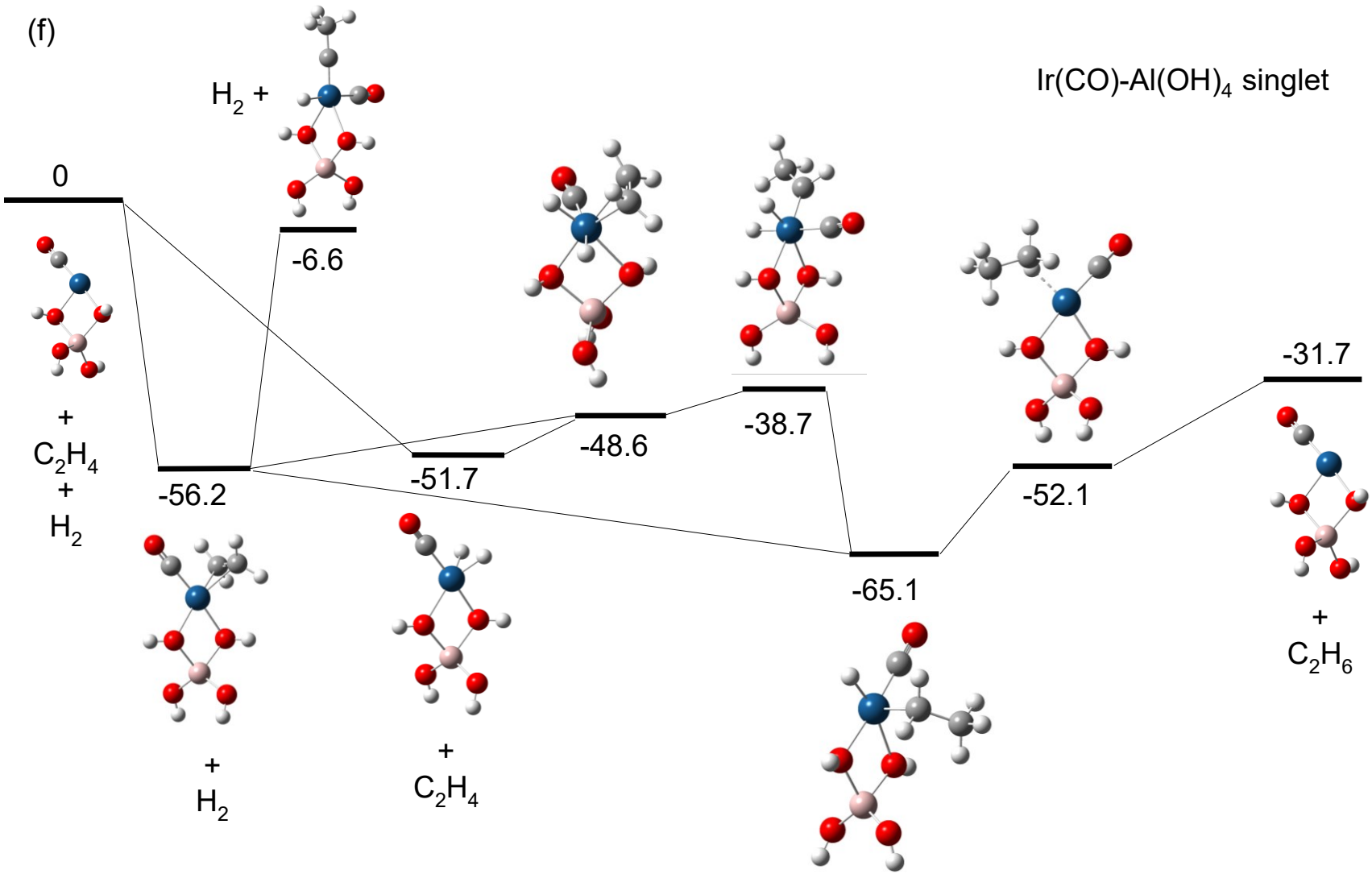

Figure 3. Potential energy surfaces with reaction energies (ΔE + ΔZPE) in kcal/mol characterizing the catalytic ethylene hydrogenation reaction on (a) Zeo(48-T)Ir at the ONIOM(B3LYP, PM6)/cc-pVDZ(-pp) level, (b) Ir–Al(OH)$_4$, singlet (values with (3) are for the triplet), (c) Ir–Al(OH)$_4$, triplet, (d) Rh–Al(OH)$_4$, singlet (values with (3) are for the triplet), (e) Co–Al(OH)$_4$, triplet, and (f) Ir(CO)–Al(OH)$_4$, singlet. Surfaces (b) – (f) are at the B3LYP/aug-cc-pVDZ(-pp) level.

reaction exothermicity of -17.1 kcal/mol, and a reaction barrier of ~25 kcal/mol. The geometry of the Ir complex with the $CHCH_3/H_2$ ligand pair has the proper orientation to eliminate C_2H_6 with the two H atoms bonded to Ir 2.20 Å away from the carbene C atom of $CHCH_3$. On another reaction path, starting from the $Ir(C_2H_4)(H_2)$ complex, a H(-Ir) can be transferred to a C of C_2H_4 to form $Ir(C_2H_5)$ with a β-H of C_2H_5 bonded to Ir, followed by the transfer of second H(-Ir) to generate C_2H_6. The transition state for the $Ir(C_2H_4)(H_2) \rightarrow Ir(\beta\text{-}C_2H_5)$ reaction was not found at the B3LYP/aug-cc-pVDZ level most likely due to the presence of a very low reaction barrier. The transition state is expected to have a geometry similar to the singlet β-H bonded $Ir(C_2H_5)(H)$ complex, which is ~15 kcal/mol higher in energy than the singlet $Ir(C_2H_4/H_2)$ complex, so the reaction barrier can be estimated to be slightly more than 15 kcal/mol. As noted previously, the inter-ligand H transfer of $Ir(C_2H_4)(H_2)$ to form $Ir(CHCH_3)(H_2)$ is expected to be comparable to the 15 kcal/mol barrier to form β-H bonded $Ir(C_2H_5)(H)$ complex, especially for the reaction based on the Zeo(48-T)Ir model. Although the reaction barriers between the intermediates of the lowest pathway on the Ir singlet PES are commonly low, formation of C_2H_6 from the intermediates is an endothermic process. The reaction step to form and release C_2H_6 from $Ir(CHCH_3)(H)$ is predicted to be 55 and 62 kcal/mol endothermic by using the $Ir–Al(OH)_4$ and the Zeo(48-T)Ir models respectively.

The adiabatic surface of the PES for the $Ir–Al(OH)_4 + C_2H_4 + H_2 \rightarrow Ir–Al(OH)_4 + C_2H_6$ basically resembles the reaction PES obtained by using the Zeo(48-T)Ir model (Figure 3a). Most of the structures shown on the $Zeo(48\text{-}T)Ir + C_2H_4 + H_2 \rightarrow Zeo(48\text{-}T)Ir + C_2H_6$ PES (Figure 3a) are singlets except for triplet Zeo(48-T)Ir. The reaction energies for the C_2H_4 and H_2 mono ligand adsoption are comparable, with the C_2H_4 reaction being 2 kcal/mol more exothermic. $Zeo(48\text{-}T)Ir(C_2H_4)$ can relax to form $Zeo(48\text{-}T)Ir(CCH_3)(H)$ with an exothermicity of ~20 kcal/mol, which can happen only if there is not a second ligand bonded to Ir. $Zeo(48\text{-}T)Ir(CHCH_3)(H_2)$ can be formed by adding H_2 to Zeo(48-T)Ir $(CCH_3)H$ or transfering H in $Zeo(48\text{-}T)Ir(C_2H_4)(H_2)$. $Zeo(48\text{-}T)Ir(CHCH_3)(H_2)$ is predicted to be ~7 kcal/mol higher in energy than $Zeo(48\text{-}T)Ir(C_2H_4)(H_2)$. The $CHCH_3/H_2$ ligand pair has closer geometry to C_2H_6 than the C_2H_4/H_2 ligand pair, and therefore $Ir(CHCH_3)(H_2)$ is likely an important intermediate in the formation of C_2H_6 catalyzed by the zeolite-supported Ir catalysts.

As noted above, the triplet states on the $C_2H_4 + H_2 + Al(OH)_4$ PES are not as stable as the singlets once ligands are added (Figure 3c). In contrast to the energetics for the singlet PES, the triplet $Ir(CHCH_3)(H_2)$ complex is ~20 kcal/mol higher in energy than the triplet $Ir(C_2H_5)(H)$ intermediate. The triplet β-H bonded $Ir(C_2H_5/H)$ is predicted to be a transition state instead of the local minimum predicted the singlet. The reaction barrier for $^3Ir(C_2H_4)(H_2) \rightarrow {}^3Ir(C_2H_5)(H)$ is predicted to be ~18 kcal/mol.

The adiabatic PES for ethylene hydrogenation on the Rh complex catalyst (Figure 3d) is mostly on the singlet surface, with triplet $Rh–Al(OH)_4$ being 10.5 kcal/mol lower in energy than the singlet and triplet $Rh(C_2H_6)–Al(OH)_4$ being 6.8 kcal/mol lower than the singlet. The singlet-triplet splittings are less than 5 kcal/mol for the first step/second adsorption products and some of the rearrangement intermediates. The reaction energy for ligand rearrangement from C_2H_4 to CCH_3/H is endothermic by 13.3 kcal/mol. $Rh(C_2H_4)(H_2)–Al(OH)_4$ can rearrange into β-H bonded $Rh(C_2H_5)(H)–Al(OH)_4$, $Rh(C_2H_5)(H)–Al(OH)_4$, $Rh(CHCH_3)(H_2)–Al(OH)_4$, and $Rh(C_2H_6)–Al(OH)_4$, with the isomerization energies of 10.6, 22.2, 19.8, and 27.4 kcal/mol, respectively. The (average) distances between the α-C atom and H(–M) in these four complexes are 2.49, 2.43, 2.18, and 1.13 Å, respectively. The crossover between the singlet and triplet PESs occurs at $Rh(C_2H_6)–Al(OH)_4$. The barrier to form β-H bonded $Rh(C_2H_5)(H)–Al(OH)_4$ is

predicted to be ~10 kcal/mol for the lowest pathway. The transition state between the β-H bonded $Rh(C_2H_5)(H)–Al(OH)_4$ and $Rh(C_2H_5)(H)–Al(OH)_4$ was not found at the B3LYP/aug-cc-pVDZ level, so the reaction barrier is the endothermicity of the conversion reaction, ~12 kcal/mol. The remaining barriers are also quite small on the singlet surface for Rh. Overall the energetics for the Rh complexes are not as negative as those for the Ir complexes.

The triplet PES is the adiabatic one for the Co complex catalyst (Figure 3e). The first excited state could be the singlet or the quintet, and the calculations predict that the quintet is normally much higher in energy than the triplet for the mono- and dual-ligand Co complexes. The only exception is that quintet $Co–Al(OH)_4$ is slightly higher in energy than the ground state (by 3.9 kcal/mol). $Co(C_2H_4)–Al(OH)_4$ could rearrange into $Co(CHCH_3)–Al(OH)_4$, but the reaction is endothermic by ~25 kcal/mol. $Co(C_2H_4)(H_2)–Al(OH)_4$ could convert into $Co(C_2H_5)(H)–Al(OH)_4$ and $Co(C_2H_6)–Al(OH)_4$, with respective reaction energies of 1.1 and -6.7 kcal/mol. The calculated distances between the α-C atom and the H atoms on Co are 2.34 Å for $Co(C_2H_5)(H)–Al(OH)_4$ and 1.13 Å for $Co(C_2H_6)–Al(OH)_4$. The energies for the Co surface are less negative than for Rh. The $Co(CHCH_3)(H_2)–Al(OH)_4$ iso-structure is not predicted to be a local minimum on the PES. The important barrier is the formation of $Co(C_2H_5)(H)–Al(OH)_4$ from $Co(C_2H_4)(H_2)–Al(OH)_4$ with a barrier of 32 kcal/mol as compared to the barriers for the rate limited steps of 10-15 kcal/mol for Rh and over 50 kcal/mol for Ir. Moreover, this barrier is now only 5 kcal/mol below the energy of the reactant asymptote. The remaining barriers are again small.

4. Discussion

4.1 Comparison of experimental and calculated vibrational frequencies

Table 2 is a summary of the available calculated and experimental results comparing IR vibrational frequencies of C–H and C≡O bonds for Ir and Rh complexes with various combinations of C_2H_4 and CO ligands on six different zeolites.[5,7,8,9,37,38] These metal complexes, including $M(C_2H_4)(C_2H_4)$, M(CO)(CO), and $M(C_2H_4)(CO)$, are among the best-characterized metal complexes on zeolite supports. It is advantageous to use these complexes for comparison because the ν_{CH} and ν_{CO} frequencies of C_2H_4 and CO ligands are sensitive to the electronic structure of the metal. The ν_{CO} frequencies of the metal carbonyl complexes are especially informative from an experimental point of view because they represent prominent features in the IR spectra.

Because the electron transfer between a CO ligand and a metal atom involves both σ donation from a p orbital of CO to a vacant d orbital of the metal and lateral π-backbonding from a filled metal d orbital to a vacant antibonding π* orbital of CO, as the electron density of a metal increases, the electron transfer from the metal to CO through π-antibonding increases, lengthening the C≡O bond and lowering its vibrational frequency. Therefore, analysis of the ν_{CO} frequencies of Rh(CO)(CO) and Ir(CO)(CO) provides the following comparison of the electron density on the metal atoms in the complexes on the six zeolites: Y < β ≈ ZSM-5 < SSZ-42 ≈ mordenite < SSZ-53. The results summarized in Table 2 show that the calculated ν_{CO} frequencies of both $Ir–Al(OH)_4$ and $Rh–Al(OH)_4$ complexes match the experimental values very well. The ν_{CO} predictions based on the $Ir–Al(OH)_4$ model are in slightly better agreement with experiment than are the predictions based on the Zeo(48-T)Ir model. This difference might be explained by the smaller basis set used in the more expensive Zeo(48-T) calculations. The results indicate that

Table 2. Comparison of Experimental and Calculated Vibrational Frequencies (cm^{-1}) of the C–H and C≡O bonds characterizing Iridium and Rhodium Complexes on Various Zeolites. [a]

Metal complex bonded to zeolite	Mode assignment	Experimental ν characterizing metal complex supported on the zeolite						DFT ν characterizing metal on zeolite	
		Y	β	SSZ-53	SSZ-42	ZSM-5	mordenite	$Al(OH)_4$/aD	Zeo/D
$Rh(C_2H_4)_2$	C–H	2979						2990	
								2991	
		3016						3001	
								3064	
		3062						3066	
		3084						3088	
								3092	
$Rh(C_2H_4)(CO)$	C–H							3003	
								3011	
								3081	
								3102	
	C≡O	2056	2048					2037	
$Rh(CO)_2$	C≡O	2052	2048		2045	2048	2045	2041	
		2117	2115		2111	2115	2111	2104	
$Ir(C_2H_4)_2$	C–H								2968
								2964	2980
									2996
								2998	3003
		3009							3060
		3022		3038				3039	3069
				3057					3084
		3082	3125					3085	3096
$Ir(C_2H_4)(CO)$	C–H	3012						2991	2988
		3023						3000	3017
		3078						3069	3082
			3118	3092				3089	3108
	C≡O	2054	2059	2041				2022	1984

$Ir(CO)_2$	C≡O	2038	2035	2027	2029			2026	1984
		2109	2106	2099	2102			2095	2050

[a] Experimental IR frequencies taken from Refs 5, 7, 8, 9, 37, and 38.

all of the experimental ν_{CO} are slightly higher than the calculated results, and the values match more closely as the electron density on the metal increases. For example, the ν_{CO} frequencies of $Ir(CO)_2$ on zeolite SSZ-53 (2027 and 2099 cm^{-1}) are only 1 and 4 cm^{-1} higher than the calculated values, respectively, whereas the ν_{CO} frequencies of the isostructural Ir complex on zeolite Y (2038 and 2109 cm^{-1}) are 12 and 14 cm^{-1} higher than the calculated values (2026 and 2095 cm^{-1}, respectively).

There are not enough available experimental results characterizing the ν_{CH} frequencies of the metal complexes to allow a comparison for the metal complexes on all six zeolites with the calculated results. Within the limits of the available results, we can conclude that the calculations generally agree very well with the experimental results characterizing the hydrocarbon ligands. For example, the scaled calculated ν_{CH} frequencies of the $Rh(C_2H_4)(C_2H_4)$ complex on zeolite Y (2990, 3001, 3066, and 3088 cm^{-1}) differ by only 11, 15, 4, and 4 cm^{-1} from the experimental values (2979, 3016, 3062, and 3084 cm^{-1}). In contrast to the intensities of the ν_{CO} bands, the intensities of the ν_{CH} bands of C_2H_4 ligands are relatively weak (more than an order of magnitude lower in intensity than the ν_{CO} bands), and therefore they are challenging to identify. Because of peak broadening, the resolved experimental bands are fewer in number than predicted by the DFT calculations. Thus, the calculated results are especially valuable for interpretation of the experimental results. The ν_{CH} predictions determined for the Ir–$Al(OH)_4$ model are generally ~10cm^{-1} lower than the predictions made with the Zeo(48-T)Ir model.

In summary, the data presented in Table 2 show good agreement between the calculated and experimental ν_{CO} and ν_{CH} frequencies. The data provide a strong justification of the simplified zeolite model used for the calculations. Moreover, the comparisons point to opportunities for future work in seeking zeolite models with parameters that can be tuned to account for the subtle differences in electron donating/withdrawing properties of the various zeolite frameworks.

4.2 Experimental confirmation of LDEs

Figure 4 shows reactions of zeolite-supported Ir and Rh complexes with CO and C_2H_4 based on analyses of transient IR and EXAFS data. [5,20] The experimental results show that all of the C_2H_4-containing complexes (i.e., $M(C_2H_4)(C_2H_4)$, $M(C_2H_4)(CO)$, and $M(C_2H_4)(C_2H_4)(CO)$) underwent fast and complete ligand exchange when brought in contact with a pulse of CO at 298 K and 1 bar, transforming each of the complexes into M(CO)(CO) without any detectable intermediates. In contrast, when M(CO)(CO) complexes were brought in contact with a continuous stream of C_2H_4, $M(CO)(CO)(C_2H_4)$ intermediate species were detected by IR spectroscopy. Moreover, treatments of M(CO)(CO) in C_2H_4 led to only partial ligand exchange, forming $M(C_2H_4)(CO)$ or $M(C_2H_4)(C_2H_4)(CO)$. These experimental observations suggest a stronger M–CO bond than M–(C_2H_4) bond for both Ir and Rh, precisely matching the calculated LDEs, which show that the single-ligand LDEs of the mono and dual-ligand complexes for CO are ~12 and ~15 kcal/mol higher in energy (when the metal is Rh) and ~17 and ~20 kcal/mol higher (when the metal is Ir) than the single-ligand LDEs of the mono and dual ligand complexes for C_2H_4, respectively. Furthermore, the calculated LDEs of C_2H_4 for Ir are significantly greater than for Rh (the differences are 25 and 15 kcal/mol for the single-ligand LDEs of the mono and dual ligand complexes, respectively), which explains the observation that when M(CO)(CO) is treated in C_2H_4, a mixture of $M(C_2H_4)(CO)$ and $M(C_2H_4)(C_2H_4)(CO)$ is formed when M = Ir, whereas when M = Rh, only $M(C_2H_4)(CO)$ is observed.

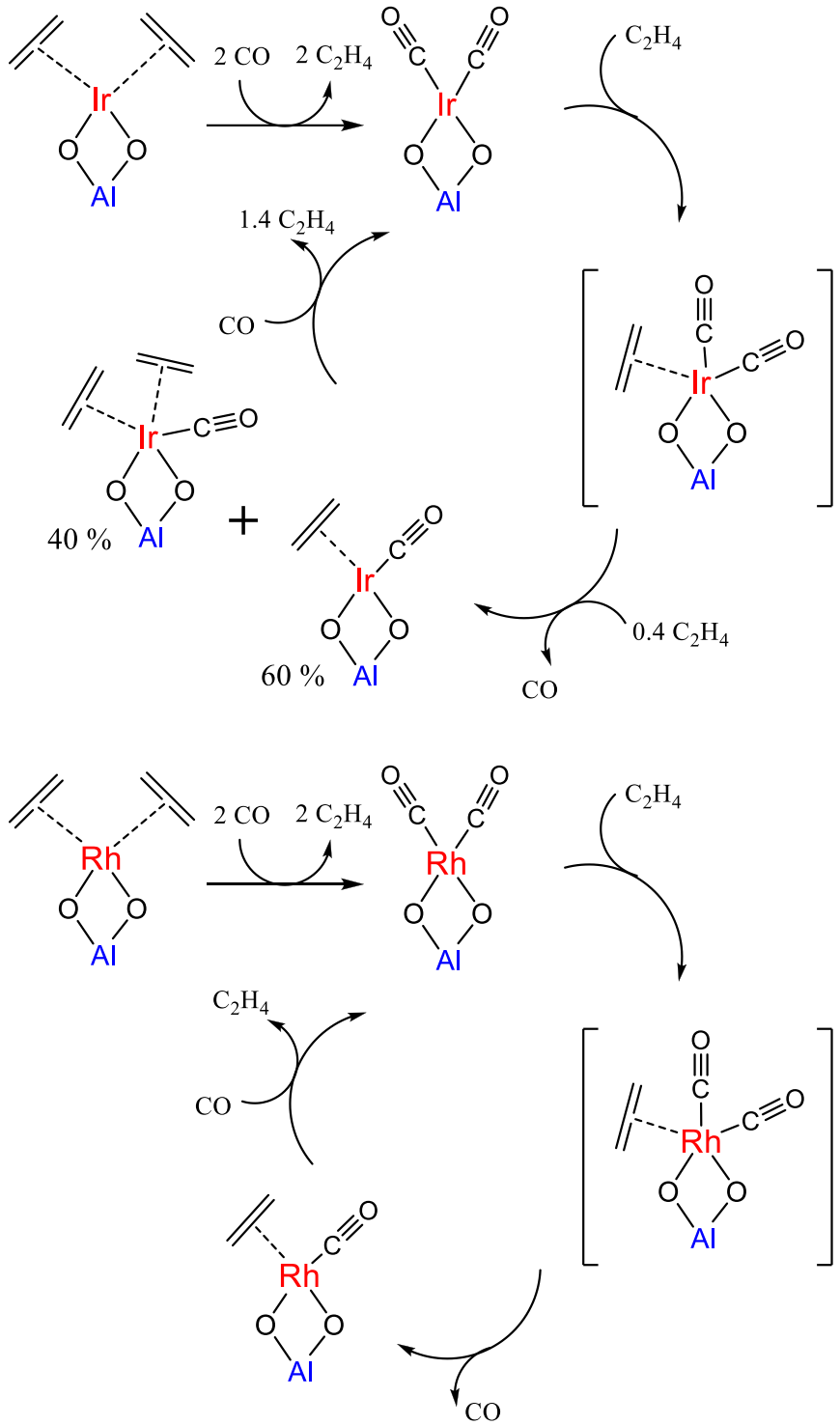

Figure 4. Experimentally determined reactions of zeolite-supported Ir and Rh complexes with CO and C_2H_4 at 298 K and 1 bar.

4.3 Metal–ethylene bonding and catalytic implications

The relative strength of back-donation between the occupied metal d and C–C π* orbitals of C_2H_4 could be the origin of the stability ordering for the metal complexes, as many of the isomerizations involve C=C or M–C bond breaking. In general, the bonding between transition metals and olefins can be explained by the Dewar-Chatt-Duncanson model.[58,59] In this model, the metal back-donates electron density from its filled d (or pd^n hybrid) orbitals into the empty olefin π*2p anti-bonding orbital, as the empty metal d orbitals perpendicular to the >C=C< plane accept electron density from the filled olefin π_{2p} orbital. The donation and back-donation lead to a reduced C–C bond order, an elongated C–C distance, and a red-shifted C–C stretching band.

The C–C and M–C bond lengths and the C–C stretching vibrational frequencies characterizing the $M(C_2H_4)(L)$–$Al(OH)_4$ complexes, for M = Co, Rh, and Ir, are given in the Supporting Information. The ordering of C–C bond lengths in the metal complexes is Ir > Rh > Co, and the ordering of the M–C bond lengths and C–C frequencies is Ir < Rh < Co. This comparison indicates stronger electron density donation between the metal and ethylene in the Ir complexes than in the Rh complexes than in the Co complexes. The only exception is $Co(C_2H_4)$–$Al(OH)_4$, which has slightly stronger bonding between the metal and the ethylene ligand than in $Rh(C_2H_4)$–$Al(OH)_4$. This result agrees well with the ordering of electrophilicities of the three metals: Ir > Rh > Co.[60]

Molecular orbital diagrams of the $M(C_2H_4)$–$Al(OH)_4$ complexes (M = Co, Rh, and Ir), show that the bonding paradigm is different from the Dewar-Chatt-Duncanson model. The bonding between the metal and ethylene is stronger than the bonding that the Dewar-Chatt-Duncanson model would suggest in all of the Rh complexes, Ir complexes, and the Co complexes $Co(C_2H_4)$–$Al(OH)_4$ and $Co(C_2H_4)(H_2)$–$Al(OH)_4$ (Supporting Information). There is electron density donated from the ethylene C–C σ orbital to the metal d orbital (denoted as σ-d donation), in addition to the π-d donation and d-π* back-donation according to the Dewar-Chatt-Duncanson model. The d-π* back-bonds are not formed in the Co complexes other than the two mentioned above, and only π-d donation is observed. One reason for the differences is that in the high-spin ground state of the Co complexes, electrons are unpaired so that they occupy more metal valence orbitals leading to increased electron repulsion in the case of back-donation from the ligand, which prevents the formation of strong d-π* back-bonds. Moreover, in the high-spin ground-state Co complexes, the ligands no longer occupy the octahedral coordination positions around the metal so that the ligand(1)–metal–ligand(2) angles are much greater than 90°. The Co d orbital in the d-π* back-bonds will be distorted by the second ligand, so that no strong d-π* overlaps can be formed. The Co d orbital is even more distorted when the ancillary ligand on the metal has an acceptor orbital that can hold the metal d electron density (e.g., CO π*). H_2 is weakly attached to Co as η^2–H_2, so it would change the electron densities in $Co(C_2H_4)(H_2)$–$Al(OH)_4$ by only a small amount, which is why $Co(C_2H_4)(H_2)$–$Al(OH)_4$ shows characteristics similar to those of $Co(C_2H_4)$–$Al(OH)_4$. The calculations show σ-d donation in most of the low-spin excited states for these Co complexes. Given the lack of d-π* back-donation, the bonds between Co and ethylene are weaker than Rh–ethylene and Ir–ethylene bonds.

The isomerization of $Co(C_2H_4)(L)$–$Al(OH)_4$ is different from those of the Rh and Ir ethylene complexes, with the carbene and carbyne complexes being less likely to form. This result is consistent with the strength of the Co–ethylene bonding. The electron densities in the C–C bonding orbitals show that they are weakly donating and strongly localized on the olefin, so that the C–C bonds are difficult to break via a homolytic process. Formation of the carbene or

carbyne complexes requires the breaking of the C–C π-bond. Moreover, H_2 is bound to Co mainly in its molecular form with extremely weak d-σ* back-donation between Co and H_2. This comparison suggests that the Co complexes are likely to be much less active catalysts than the Ir and Rh complexes for C–C and H–H activations, as the ligands in the Co complexes maintain their molecular characters. The ethylene hydrogenation reaction on the Co catalyst is likely to have a higher energy barrier if the reaction follows a path whereby H_2 dissociates and then H is added to the C–C bond. Co(Z-but-2-ene)–$Al(OH)_4$ could possibly be formed from $Co(C_2H_4)(C_2H_4)$–$Al(OH)_4$ with the attribution of the π-π conjugation between two ethylene ligands, followed by the hydrogen transfer of the ligands, and, again, the driving force is not C–C bond breaking.

In contrast, the Ir–ethylene bonds are relatively strong, and a full rupture of the Ir–ethylene bonds will be highly endothermic and thus difficult. Nevertheless, the strong σ-d, π-d, and d-π* donations make the Ir–ethylene bonds overpopulated with electron density, so that the electron density will tend to be reallocated. A back-bond between Ir d and ethylene π* orbitals has two segments that are the overlaps of electron densities between Ir and each of the two C atoms. During the catalytic reaction, one of the d-π* back-donation segments could be strengthened as the other segment decomposes. These changes lead to the formation of an Ir–C σ-bond between the Ir d-orbital and C p-orbital, and a nascent acidic center is created, which can induce hydrogen transfer reactions. This inference explains why the Ir carbene/carbyne complexes are low-lying isomers or even the lowest-energy isomers. If the donation and back-donation of electron densities between ethylene and the metal are strong enough, even the C–C bonds can be broken, forming complexes like $M(CH_2)(CH_2)$–$Al(OH)_4$ and $M(CH_2)(C_3H_6)$–$Al(OH)_4$, in which the back-donation bond is converted into two M–C sigma bonds.

Rh–ethylene bonds are weaker than the Ir–ethylene bonds but stronger than the Co–ethylene bonds, and they exhibit intermediate characteristics. Because ethylene activation on the metal catalysts is largely related to the ability of the metal sites to create acidic centers, the Ir complexes should perform better than the Rh complexes for ethylene activation. This inference is consistent with the experimental observation of a much higher catalytic ethylene hydrogenation rate on the zeolite Y-supported Ir catalyst than on the zeolite Y-supported Rh catalyst.[16,18]

The catalytic activities for ethylene hydrogenation and H_2 dissociation of $Ir(C_2H_4)(C_2H_4)$ complexes on two different zeolites (Y and SSZ-53) were reported recently.[7] These experimental results led to the conclusion that when Ir is bonded to the acidic zeolite, C_2H_4 activation is rate-limiting for ethylene hydrogenation. This situation is contrasted with that when the support is the electron-donating MgO, for which H_2 activation is rate-limiting.[16] Furthermore, the $Ir(C_2H_4)_2$ complex is more electron deficient when bonded to zeolite Y than to SSZ-53, which leads to a stronger interaction between the Ir atom and C_2H_4 ligands and thus a higher activity for ethylene hydrogenation. The DFT/ONIOM predictions show that the LDE(H_2) is only 2.2 kcal/mol (6.6 kcal/mol with the simple model) less than LDE(C_2H_4) for the according model iridium complexes. Moreover, the activation barrier is hypothesized to be low because of the strong interaction between Ir and the atoms (C's and H's) in the ligand attached to Ir. The results suggest that it is possible to change the activation energy by altering the support material. The different predictions for the (LDE(C_2H_4) - LDE(H_2)) using the Zeo(48-T)Ir and Ir–$Al(OH)_4$ models are mainly attributed to the larger steric effect with the Zeo(48-T)Ir model, which suggests the size of the supercages in the support can also have an influence on the rate-limiting step.

4.4 Potential Energy Surfaces

For the ethylene hydrogenation reactions (on the bare metal catalysts) discussed in section 3.7, the first-step adsorption of C_2H_4 is more exothermic than that of H_2 for all three metals, but the differences between the LDEs of C_2H_4 and H_2, which are equivalent to the energy differences between the first-step adsorptions and also ligand exchange energies, are markedly different for the three metals. The C_2H_4–H_2 ligand exchange energy is only 6.6 kcal/mol for the reaction with the Ir complex; 13.4 kcal/mol for Rh; and 30.9 kcal/mol for Co, which will impact the direction in which the reaction will proceed.

Another difference in the potential energy surfaces of the three metals is the energetic ordering of the isomers of $M(C_2H_4)(H_2)$–$Al(OH)_4$. The ordering is $C_2H_4/H_2 < CHCH_3/H_2 << {}^3C_2H_5/H << {}^3C_2H_6$ for Ir, $C_2H_4/H_2 << CHCH_3/H_2 \approx C_2H_6 \approx C_2H_5/H$ for Rh, and $C_2H_6 < C_2H_4/H_2 \approx C_2H_5/H < CHCH_3/H_2$ (rearranged) for Co. This comparison suggests that as the metal is changed from Ir to Co, the selectivity of the isomerization changes dramatically, and the reaction path will favor $M(C_2H_6)$–$Al(OH)_4$ and not favor $M(C_2H_4)(H_2)$–$Al(OH)_4$ and $M(CHCH_3)(H_2)$–$Al(OH)_4$.

The differences in the stabilities of the intermediates on the PES's for M = Ir, Rh, and Co lead to markedly different predicted mechanisms for the C_2H_4 hydrogenation reaction on these M-zeolite catalysts; specifically, the reaction step that determines the rate of the C_2H_4 hydrogenation differs for the three metals. For Rh, all of the steps including the step to form C_2H_6 on the lowest-energy reaction pathway are predicted to have comparable small barriers of 10–15 kcal/mol. For Co, the step for conversion of the $Co(C_2H_4)(H_2)$ intermediate to the $Co(C_2H_5)(H)$ intermediate has the highest barrier. For Ir, the last step of the catalytic cycle, formation and release of C_2H_6, is the one that controls the rate of reaction. The reaction PES for Ir shows that the intermediates are very stable, so that there is a much larger barrier to eliminate the C_2H_6. The energy to release C_2H_6 decreases from Ir to Rh to Co. If a surface crossing can occur from the singlet to triplet in the exit channel, the energy to form C_2H_6 is only 3 kcal/mol for Rh. On the triplet surface for Co, this energy to release C_2H_6 is 12 kcal/mol. On the Ir surface, this energy is closer to ~55 kcal/mol. Our results suggest that the zeolite-supported Rh catalyst may be the most active of the three as it will require the least excess energy to overcome any energy barriers; the elimination of C_2H_6 from the intermediate should be relatively facile; and the well depths characterizing the intermediates are not as great as for Ir. The barriers on the lowest-energy reaction pathways of the Ir PES are also of moderate magnitude, but the release of C_2H_6 from the Ir catalyst requires a larger excess energy as compared to the Rh and Co catalysts as a consequence of the stabilities of the intermediates. The stability and variety of the Ir intermediates are of interest in terms of potential trapping of observable intermediates, and their manipulation may be useful in directing different synthetic pathways.

As the calculated LDE results show, Ir forms the strongest M-ethylene and M-H_2 bonds among the three metals. The stronger Ir-C and Ir-H bonds leads to an effective weakening of the C=C and H-H bonds in ethylene and H_2, respectively. This has two implications in the catalysis of the ethylene hydrogenation reactions: 1) the Ir catalyst can most efficiently activate the adsorbed ethylene and hydrogen; and 2) it is more difficult for the Ir catalyst to release the hydrogenation product C_2H_6. The well depth of the Ir PES is deeper than that of the Rh and Co PES's, which is consistent with the two catalytic implications. Experimentally, the Ir catalyst has better performance than the Rh catalyst for ethylene hydrogenation reactions. Our results are consistent with this as the C_2H_6 can be readily displaced by an incoming ligand such as C_2H_4 or

CO (See Figure 3b and 3f).

It is important to note that the calculated reaction PES is based on a tetra-coordinate MX_4 (M = Co, Rh, Ir, and X = silicate, H_2, C_2H_4, C_2H_5, etc) geometry, which is best describes the reaction when the acidic site adsorbs one ethylene only. The zeolite supported Group 9 catalysts can have a strong σ donor ligand (CO) bonded to the metal as the auxiliary ligand if $M(CO)_2$(acac) was used to synthesize the catalyst as the precursor. The CO auxiliary ligand will weaken the backbonding between M and the C=C or H–H of the co-existing ligands. The reaction mechanism could differ when two ethylene ligands have been adsorbed (or one auxiliary ligand and one ethylene), in which cases the reaction is based on the octahedral coordination (MX_6, where X = silicate, H, C_2H_4, C_2H_5, etc). The MX_6 reaction is not discussed in detail in the current work and a systematic study of the MX_6 reactions with different auxiliary ligands on the metal is currently ongoing. Figure 3f shows the thermodynamics of the ethylene hydrogenation reaction on Ir(CO)–$Al(OH)_4$, where the Ir mostly has MX_5 or MX_6 coordination. The exothermicities of the initial adsorption reactions to form Ir(CO)(C_2H_4)–$Al(OH)_4$ and Ir(CO)(H_2)–$Al(OH)_4$ are comparable to the exothermicities of the initial adsorption reactions on Ir–$Al(OH)_4$. The formation of Ir(CO)(C_2H_4)–$Al(OH)_4$ is more favorable by 4.5 kcal/mol than the formation of Ir(CO)(H_2)–$Al(OH)_4$, as compared to the energy difference of 8.2 kcal/mol on Ir–$Al(OH)_4$. The PES with the Ir–$Al(OH)_4$ precursor shows that Ir(C_2H_4)(H_2)–$Al(OH)_4$ is a stable intermediate for the ethylene hydrogenation reaction. This is not the case for the ethylene hydrogenation reaction on Ir(CO)–$Al(OH)_4$, where the formation of Ir(CO)(C_2H_4)(H_2) from the first-step adsorption products are endothermic. Instead, Ir(CO)(C_2H_5)(H)–$Al(OH)_4$ is found to be the only structure that is formed from the Ir(CO)(C_2H_4)–$Al(OH)_4$ + H_2 reaction. This result is consistent with the suggestion that Ir(C_2H_5)(H) is a reaction intermediate for the ethylene hydrogenation reaction on the zeolite supported iridium catalyst on the basis of experimental studies.[16,27] The well depth of the ethylene hydrogenation reaction is calculated to be ~65 kcal/mol on Ir(CO)–$Al(OH)_4$, much smaller than the well depth (~105 kcal/mol) when the auxiliary CO ligand is absence, but still a significant stabilization. The Ir(CO)(C_2H_6)–$Al(OH)_4$ complex where C_2H_6 is bonded to Ir(CO)–$Al(OH)_4$ by a Ir-H(C) bond, is formed from Ir(CO)(C_2H_5)(H)–$Al(OH)_4$ by an endothermic reaction with ΔH = 13 kcal/mol. Clearly, the existence of the auxiliary CO ligand reduces the excess energy required to form ethane. The isomers with the carbene and carbyne ligands are predicted to be energetically unfavorable on Ir(CO)–$Al(OH)_4$, even though some of these isomers are vibrationally stable (local minima).

4. Conclusions

Two computational models of different sizes were used to characterize ligand properties and dissociation energetics of zeolite-supported Group 9 transition metal complex catalysts. The simple M^+–$Al(OH)_4^-$ model provided geometries, vibrational frequencies, and LDEs characterizing the zeolite-supported Group 9 transition metal catalysts that are consistent with the limited amount of available experimental values for Rh and Ir and with the computational results based on the ONIOM calculations determined using the much larger Zeo(48-T)Ir model. The use of the $Al(OH)_4M$ model greatly reduced the computational cost—yet still retained most of the key energetic features for the simulation of the Group 9 transition metal complex catalysts in a zeolite environment. In addition, the use of the -D3 dispersion corrected functional[33] did not substantially change the results for the Co complexes.

The ground-state structures of Co(L_1)(L_2)$Al(OH)_4$ complexes tend to be high-spin and have

non-planar ligand coordination as a consequence of the tetrahedral ligand field, whereas most of the ground-state structures of $Rh(L_1)(L_2)Al(OH)_4$ and $Ir(L_1)(L_2)Al(OH)_4$ complexes are low-spin and have planar geometry in an octahedral ligand field. The differences between the geometry and stability of the Co complexes, and the Rh and Ir complexes, are related to the low-lying electronic states of the Co^+, Rh^+, and Ir^+ ions.

Binding of common ligands from the gas phase to the model structure $M–Al(OH)_4$ (M = Co, Rh, Ir) was investigated by using DFT, including calculations of the LDEs, NBO charges, and vibrational frequencies. The calculated ligand dissociation energies show that the metal–ligand interaction strength has the following order: LDE(Ir–L) > LDE(Rh–L) > LDE(Co–L). The strength of the M–L bond is related to the electron density distribution in the ligand, which affects the reactivities in ligand activation reactions on the transition metal complex catalysts. Carbyne and carbene ligands, which are potential intermediates in the observed organic ligand activations, were found to be more stable on the Ir complexes than on the Rh or Co complexes. The results suggest that the Ir complex catalyst should be the best for C=C and H–H bond activation in terms of generating stable intermediates. The relative values of the calculated LDEs are consistent with the experimental results determined in transient IR and EXAFS experiments characterizing the Ir and Rh complexes with CO and C_2H_4. Good agreement was also found between the calculated and experimental νCO and νCH frequencies. The computational results provide the first reasonable estimates of these quantities for these types of single-site catalysts, and they can be used to improve catalyst design.

The potential energy surfaces were calculated for the ethylene hydrogenation reaction catalyzed by the Ir, Rh, and Co complexes. The PES for the ethylene hydrogenation reaction on Ir has the deepest well depth among the three metals, implying that the Ir catalyst has the best performance in activation consistent with the experimental observation that Ir is more active than Rh. The zeolite supported Group 9 catalysts can have a CO bonded to the metal as the auxiliary ligand if $M(CO)_2(acac)$ was used as the precursor in the synthesis. For the hydrogenation reaction on the Ir catalysts, the auxiliary CO ligand can lower the stability of the various reaction intermediates, reduce the reaction barrier (which is correlated to the well depth) to release C_2H_6, and consequently improve the reaction efficiency. The ethylene hydrogenation PES largely depends on the electrophilicity of the isolated M site (with or without auxiliary ligands), which determines the M-C and M-H bond strengths. The reactivity of the hydrogenation reaction can be improved by the choice of the metal, supports, and auxiliary ligands. Overall, the computational results together with the experimental observations provide a relatively complete picture of the catalytic hydrogenation of ethylene on single-site supported Rh and Ir catalysts and provide suggestions as to what to observe in future experimental investigations.

Acknowledgments.

This work was supported by the Chemical Sciences, Geosciences, and Biosciences Division, Office of Basic Energy Sciences, U.S. Department of Energy (DOE) under grant no. DE-SC0005822 (catalysis center program). DAD thanks the Robert Ramsay Chair Fund of The University of Alabama for support. MC was partially sponsored by the Oak Ridge Leadership Computing Facility at the Oak Ridge National Laboratory, which is supported by the Office of Science of the U.S. Department of Energy under Contract No. DE-AC05-00OR22725.

Notes and References

[1] A. Labouriau, G. Panjabi, B. Enderle, T. Pietrass, B. C. Gates, W. L. Earl, K. C. Ott, ^{129}Xe NMR Spectroscopy of Metal Carbonyl Clusters and Metal Clusters in Zeolite NaY. J. Am. Chem. Soc. 121 (1999) 7674–7681.

[2] F. Li, B.C. Gates, Size-Dependent Catalytic Activity of Zeolite-Supported Iridium Clusters. J. Phys. Chem. C, 111 (2007) 262–267.

[3] I. Ogino, B.C. Gates, Molecular Chemistry in a Zeolite: Genesis of a Zeolite Y-Supported Ruthenium Complex Catalyst. J. Am. Chem. Soc. 130 (2008) 13338–13346.

[4] I. Ogino, B.C. Gates, Transient Spectroscopic Characterization of the Genesis of a Ruthenium Complex Catalyst Supported on Zeolite Y. J. Phys. Chem. C 113 (2009) 20036–20043.

[5] I. Ogino, B.C. Gates, Reactions of Highly Uniform Zeolite H-β-Supported Rhodium Complexes: Transient Characterization by Infrared and X-ray Absorption Spectroscopies. J. Phys. Chem. C 114 (2010) 8405-8413.

[6] I. Ogino, B.C. Gates, Essentially Molecular Metal Complexes Anchored to Zeolite β: Synthesis and Characterization of Rhodium Complexes and Ruthenium Complexes Prepared from $Rh(acac)(\eta^2\text{-}C_2H_4)_2$ and cis-$Ru(acac)_2(\eta^2\text{-}C_2H_4)_2$. J. Phys. Chem. C 114 (2010) 2685-2693.

[7] J. Lu, C. Aydin, A.J. Liang, C.-Y. Chen, N.D. Browning, B.C. Gates, Site-Isolated Molecular Iridium Complex Catalyst Supported in the 1-Dimensional Channels of Zeolite HSSZ-53: Characterization by Spectroscopy and Aberration-Corrected Scanning Transmission Electron Microscopy. ACS Catal. 2 (2012) 1002-1012.

[8] A.J. Liang, V.A. Bhirud, J.O. Ehresmann, P.W. Kletnieks, J.F. Haw, B.C. Gates, A Site-Isolated Rhodium−Diethylene Complex Supported on Highly Dealuminated Y Zeolite: Synthesis and Characterization. J. Phys. Chem. B 109 (2005) 24236-24243.

[9] A. Uzun, V.A. Bhirud, P.W. Kletnieks, J.F. Haw, B.C. Gates, A Site-Isolated Iridium Diethylene Complex Supported on Highly Dealuminated Y Zeolite: Synthesis and Characterization. J. Phys. Chem. C 111 (2007) 15064-15073.

[10] A.J. Liang, B.C Gates, Time-Resolved Structural Characterization of Formation and Break-up of Rhodium Clusters Supported in Highly Dealuminated Y Zeolite. J. Phys. Chem. C 112 (2008) 18039–18049.

[11] T.J. Lee, B.C. Gates, Rhodium in Basic Zeolite Y: A Stable, Selective Catalyst for CO Hydrogenation. J. Mol. Catal. 71 (1992) 335-346.

[12] B.D. Vineyard, K.S. Knowles, M.J. Sabacky, G.L. Bachman, D.J. Weinkauff, Asymmetric Hydrogenation. Rhodium Chiral Bisphosphine Catalyst. J. Am. Chem. Soc. 99 (1977) 5946–5952.

[13] D.A. Colby, R.G. Bergman, J.A. Ellman, Rhodium-Catalyzed C−C Bond Formation via Heteroatom-Directed C−H Bond Activation. Chem. Rev. 110 (2010) 624-655.

[14] M. Feller, Y. Diskin-Posner, L.J.W. Shimon, E. Ben-Ari, D. Milstein, N–H Activation by Rh(I) via Metal–Ligand Cooperation. Organomet. 31 (2012) 4083-4101.

[15] E. Ben-Ari, G. Leitus, L.J.W. Shimon, D. Milstein, Metal−Ligand Cooperation in C−H and H_2 Activation by an Electron-Rich PNP Ir(I) System: Facile Ligand Dearomatization−Aromatization as Key Steps. J. Am. Chem. Soc. 128 (2006) 15390–15391

[16] J. Lu, P. Serna, C. Aydin, N.D. Browning, B.C. Gates, Supported Molecular Iridium Catalysts: Resolving Effects of Metal Nuclearity and Supports as Ligands. J. Am. Chem. Soc. 133 (2011) 16186-16195.

[17] P. Serna, B.C. Gates, Zeolite-Supported Rhodium Complexes and Clusters: Switching Catalytic Selectivity by Controlling Structures of Essentially Molecular Species. J. Am. Chem. Soc. 133 (2011) 4714-4717.

[18] P. Serna, B.C. Gates, A Bifunctional Mechanism for Ethene Dimerization: Catalysis by Rhodium Complexes on Zeolite HY in the Absence of Halides. Angew. Chem. Int. Ed. 50 (2011) 5528-5531.

[19] P.W. Kletnieks, A.J. Liang, R. Craciun, J.O. Ehresmann, D.M. Marcus, V.A. Bhirud, M.M. Klaric, M.J. Hayman, D.R. Guenther, O.P. Bagatchenko, D.A. Dixon, B.C. Gates, J.F. Haw, Molecular Heterogeneous Catalysis: A Single-Site Zeolite-Supported Rhodium Complex for Acetylene Cyclotrimerization. Chem.--Eur. J. 13 (2007) 7294-7304.

[20] A.J. Liang, R. Craciun, M. Chen, T.G. Kelly, P.W. Kletnieks, J.F. Haw, D.A. Dixon, B.C. Gates, Zeolite-Supported Organorhodium Fragments: Essentially Molecular Surface Chemistry Elucidated with Spectroscopy and Theory. J. Am. Chem. Soc. 131 (2009) 8460-8473.

[21] K.I. Hadjiivanov, G.N. Vayssilov, CO as a Probe Molecule in the Characterization of Oxide Surfaces and Zeolites. Adv. Catal. 47 (2002) 307–511.

[22] D. Astruc, Organometallic Chemistry and Catalysis; Springer: Berlin, Heidelberg, New York, 2007.

[23] J.F. Goellner, B.C. Gates, G.N. Vayssilov, N. Rösch, Structure and Bonding of a Site-Isolated Transition Metal Complex: Rhodium Dicarbonyl in Highly Dealuminated Zeolite Y. J. Am. Chem. Soc. 122 (2000) 8056-8066.

[24] I. Ogino, M. Chen, J. Dyer, P.W. Kletnieks, J.F. Haw, D.A. Dixon, B.C. Gates, A Zeolite-supported Molecular Ruthenium Complex with η^6-C_6H_6 Ligands: Chemistry Elucidated by Using Spectroscopy and Density Functional Theory. Chem.–Eur. J. 16 (2010) 7427-7436.
[25] D. Yang, M. Chen, C. Martinez-Macias, D.A. Dixon, B.C. Gates, Mononuclear Iridium Dinitrogen Complexes Bonded to Zeolite HY. Chem.–Eur. J. 21 (2015) 631–640
[26] C. Baerlocher, L.B. McCusker, D.H. Olson, Atlas of Zeolite Framework Types. 6th Edition, Structure Commission of the International Zeolite Association. Elsevier: Amsterdam, Oxford, 2007.
[27] C. Martinez-Macias, M. Chen, D.A. Dixon, B.C. Gates, Single-Site Zeolite-Anchored Organoiridium Carbonyl Complexes: Characterization of Structure and Reactivity by Spectroscopy and Computational Chemistry. Chem.–Eur. J. 21 (2015) 11825–11835.
[28] C. Lee, W. Yang, R.G. Parr, Development of the Colle-Salvetti correlation-energy formula into a functional of the electron density, Phys. Rev. B 37 (1988) 785-789.
[29] B. Miehlich, A. Savin, H. Stoll, H. Preuss, Results Obtained with the Correlation Energy Density Functionals of Becke and Lee, Yang and Parr. Chem. Phys. Lett. 157 (1989) 200-206.
[30] A.D. Becke, Density-functional thermochemistry. III. The role of exact exchange, J. Chem. Phys. 98 (1993) 5648-5652.
[31] R.A. Kendall, T.H. Dunning, R.J. Harrison, Electron affinities of the first-row atoms revisited. Systematic basis sets and wave functions, J. Chem. Phys. 96 (1992) 6796-6806.
[32] D. Figgen, K.A. Peterson, M. Dolg, H. Stoll, Energy-consistent pseudopotentials and correlation consistent basis sets for the 5d elements Hf–Pt, J. Chem. Phys. 130 (2009) 164108 (5 pages).
[33] S. Grimme, J. Antony, S. Ehrlich and H. Krieg, A Consistent and Accurate Ab Initio Parameterization of Density Functional Dispersion Correction (DFT-D) for the 94 Elements H-Pu, J. Chem. Phys. 132 (2010) 154104.
[34] S. Dapprich, I. Komáromi, K.S. Byun, K. Morokuma, M.J. Frisch, A New ONIOM Implementation in Gaussian 98. 1. The Calculation of Energies, Gradients and Vibrational Frequencies and Electric Field Derivatives. J. Mol. Struct. (Theochem) 462 (1999) 1-21.
[35] T.H. Dunning, Gaussian Basis Sets for Use in Correlated Molecular Calculations. I. The Atoms Boron Through Neon and Hydrogen, J. Chem. Phys. 90 (1989) 1007-1023.
[36] M.J. Frisch, G.W. Trucks, H.B. Schlegel, G.E. Scuseria, M.A. Robb, J.R. Cheeseman, G. Scalmani, V. Barone, B. Mennucci, G.A. Petersson, H. Nakatsuji, M. Caricato, X. Li, H.P. Hratchian, A.F. Izmaylov, J. Bloino, G. Zheng, J.L. Sonnenberg, M. Hada, M. Ehara, K. Toyota, R. Fukuda, J. Hasegawa, M. Ishida, T. Nakajima, Y. Honda, O. Kitao, H. Nakai, T. Vreven, J. Montgomery, J. A., J.E. Peralta, F. Ogliaro, M. Bearpark, J.J. Heyd, E. Brothers, K.N. Kudin, V.N. Staroverov, R. Kobayashi, J. Normand, K. Raghavachari, A. Rendell, J.C. Burant, S.S. Iyengar, J. Tomasi, M. Cossi, N. Rega, N.J. Millam, M. Klene, J.E. Knox, J.B. Cross, V. Bakken, C. Adamo, J. Jaramillo, R. Gomperts, R.E. Stratmann, O. Yazyev, A.J. Austin, R. Cammi, C. Pomelli, J.W. Ochterski, R.L. Martin, K. Morokuma, V.G. Zakrzewski, G.A. Voth, P. Salvador, J.J. Dannenberg, S. Dapprich, A.D. Daniels, Ö. Farkas, J.B. Foresman, J.V. Ortiz, J. Cioslowski, D.J. Fox, Gaussian 09, Revision D.1, Gaussian, Inc., Wallingford CT, 2009
[37] I. Ogino, C.-Y. Chen, B.C. Gates, Zeolite-supported Metal Complexes of Rhodium and of Ruthenium: a General Synthesis Method Influenced by Molecular Sieving Effects. Dalton Trans. 39 (2010) 8423-8431.
[38] J. Lu, C. Aydin, N.D. Browning, B.C. Gates, Oxide- and Zeolite-supported Isostructural $Ir(C_2H_4)_2$ Complexes: Molecular-level Observations of Electronic Effects of Supports as Ligands. Langmuir 28 (2012) 12806-12815.
[39] F. Weinhold, in Encyclopedia of Computational Chemistry; P. v. R. Schleyer, Ed.; John Wiley & Sons: Chichester, U.K., 1998, Vol. 3, pp 1792−1811.
[40] F. Weinhold, C. R. Landis, Valency and Bonding: A Natural Bond Orbital Donor-Acceptor Perspective; University Press: Cambridge, U.K., 2003.
[41] A.E. Reed, L.A. Curtiss, F. Weinhold, Intermolecular Interactions from a Natural Bond Orbital, Donor-acceptor Viewpoint. Chem. Rev. 88 (1988) 899-926.
[42] A.E. Reed, R.B. Weinstock, F. Weinhold, Natural population analysis. J. Chem. Phys. 83 (1985) 735-746.
[43] S. Li, H.-J. Zhai, L.-S. Wang, D.A. Dixon, Structural and Electronic Properties of Reduced Transition Metal Oxide Clusters, M_3O_8 and $M_3O_8^-$ (M = Cr, W), from Photoelectron Spectroscopy and Quantum Chemical Calculations. J. Phys. Chem. A 113 (2009) 11273-11288.
[44] S. Li, H.-J. Zhai, L.-S. Wang, D.A. Dixon, Structural and Electronic Properties of Reduced Transition Metal Oxide Clusters, M_4O_{10} and $M_4O_{10}^-$ (M = Cr, W), from Photoelectron Spectroscopy and Quantum Chemical Calculations. J. Phys. Chem. A 116 (2012) 5256-5271.
[45] B.N. Figgis, M.A. Hitchman, Ligand Field Theory and Its Applications, Wiley VCH, New York, 2000, 215-218.

[46] A.M. Ricks, J.M. Bakker, G.E. Douberly, M.A. Duncan, Infrared Spectroscopy and Structures of Cobalt Carbonyl Cations, $Co(CO)_n^+$ (n = 1−9). J. Phys. Chem. A 113 (2009) 4701-4708.
[47] B. von Ahsen, C. Bach, M. Berkei, M. Köckerling, H. Willner, G. Hägele, F. Aubke, Cationic Carbonyl Complexes of Rhodium(I) and Rhodium(III): Syntheses, Vibrational Spectra, NMR Studies, and Molecular Structures of Tetrakis(carbonyl)rhodium(I) Heptachlorodialuminate and -gallate, $[Rh(CO)_4][Al_2Cl_7]$ and $[Rh(CO)_4][Ga_2Cl_7]$. Inorg. Chem. 42 (2003) 3801-3814.
[48] J.E. Sansonetti, W.C. Martin, Handbook of Basic Atomic Spectroscopic Data. J. Phys. Chem. Ref. Data 34 (2005) 1559-2254.
[49] K.P. Huber, G. Herzberg, Molecular Spectra and Molecular Structure. IV. Constants of Diatomic Molecules. Van Nostrand Reinhold: New York, 1979.
[50] G.J. Kubas, J. Organomet. Chem. 635 (2001) 37-68.
[51] D. Yardimci, P. Serna, B.C. Gates, Tuning Catalytic Selectivity: Zeolite- and Magnesium Oxide-Supported Molecular Rhodium Catalysts for Hydrogenation of 1,3-Butadiene, ACS Catal. 2 (2012) 2100−2113.
[52] J. Lu, P. Serna, B.C. Gates, Zeolite- and MgO-Supported Molecular Iridium Complexes: Support and Ligand Effects in Catalysis of Ethene Hydrogenation and H–D Exchange in the Conversion of $H_2 + D_2$. ACS Catal. 1(2011) 1549-1561.
[53] J. Lu, C. Aydin, N.D. Browning, B.C. Gates, Hydrogen Activation and Metal Hydride Formation Trigger Cluster Formation from Supported Iridium Complexes. J. Am. Chem. Soc. 134 (2012) 5022-5025.
[54] S.H. Strauss, D.F. Shriver, Lewis Acid-influenced Ethylene Hydrogenation by Rhodium(I) Complexes. Inorg. Chem. 17 (1978) 3069-3074.
[55] M. Vasiliu, S. Li, A.J. Arduengo, D.A. Dixon, Bond Energies in Models of the Schrock Metathesis Catalyst. J. Phys. Chem. C 115 (2011) 12106–12120.
[56] T. Shimanouchi, Tables of Molecular Vibrational Frequencies. Consolidated Volume I, Natl. Stand. Ref. Data Ser. 39, US Natl. Bur. Stand., Washington, DC, 1967.
[57] J.B. Pedley, Thermochemical Data and Structures of Organic Compounds, TRC Data Series, Thermodynamics Research center, College Station, TX, 1994; Vol 1.
[58] M.J.S. Dewar, A review of π Complex Theory. Bull. Soc. Chim. Fr. 18 (1951) C71-C79.
[59] J. Chatt, L.A. Duncanson, Olefin Co-ordination Compounds. Part III. Infra-red Spectra and Structure: Attempted Preparation of Acetylene Complexes. J. Chem. Soc. 1953 2939-2947.
[60] R.G. Parr, L.V. Szentpály, S. Liu, Electrophilicity Index. J. Am. Chem. Soc. 121 (1999) 1922-1924.